applied sciences

MDPI

Article

System-Level Assessment of Massive Multiple-Input–Multiple-Output and Reconfigurable Intelligent Surfaces in Centralized Radio Access Network and IoT Scenarios in Sub-6 GHz, mm-Wave, and THz Bands

João Pedro Pavia [1,2], Vasco Velez [2,3], Nuno Souto [2,3], Mário Marques da Silva [2,4,*] and Américo Correia [2,3]

[1] Department of Applied Digital Technologies, ISCTE-Instituto Universitário de Lisboa, 1649-026 Lisbon, Portugal; joao.pedro.pavia@iscte-iul.pt
[2] Instituto de Telecomunicações, 1049-001 Lisbon, Portugal; vasco_velez@iscte-iul.pt (V.V.); nuno.souto@iscte-iul.pt (N.S.); americo.correia@iscte-iul.pt (A.C.)
[3] Department of Information Science and Technology, ISCTE-Instituto Universitário de Lisboa, 1649-026 Lisbon, Portugal
[4] Department of Engineering and Computer Science, Universidade Autónoma de Lisboa, 1169-023 Lisbon, Portugal
* Correspondence: mmsilva@autonoma.pt

Abstract: In this article, we investigate in different scenarios the feasibility of using massive multiple-input–multiple-output (mMIMO) with reconfigurable intelligent surfaces (RISs) to increase the throughput and coverage with high energy efficiency, considering sub-6 GHz, mmWave, and THz bands. With that objective, a centralized radio access network (C-RAN) suitable for beyond fifth-generation (B5G) systems is considered, where we integrate the base stations (BSs) with multiple RISs and IoT devices or user equipment. RISs with a large number of quasi-passive reflecting elements constitute a low-cost approach capable of shaping radio wave propagation and improving wireless connectivity. We consider a scenario where multiple RISs are combined with mMIMO in the uplink in order to provide connectivity to a smart city (with thousands of active low-power IoT devices), wirelessly, in the 3.6 GHz and 28 GHz bands. We also address a scenario where RISs are adopted with mMIMO in the downlink so as to offer connectivity to a stadium with a pitch, (and thousands of active users' equipment) in the 28 GHz band. Finally, we also studied the connectivity at 100 GHz of a factory in which several RIS panels, replacing most of the BSs equipped with mMIMO, assure improved throughput and coverage. We concluded that RISs are capable of improving the performance in any of these analyzed scenarios at the different frequency bands, justifying that they are a key enabling technology for 6G.

Keywords: RIS; massive MIMO; system-level simulation; C-RAN; precoding; B5G; IoT

Citation: Pavia, J.P.; Velez, V.; Souto, N.; Silva, M.M.d.; Correia, A. System-Level Assessment of Massive Multiple-Input–Multiple-Output and Reconfigurable Intelligent Surfaces in Centralized Radio Access Network and IoT Scenarios in Sub-6 GHz, mm-Wave, and THz Bands. *Appl. Sci.* **2024**, *14*, 1098. https://doi.org/10.3390/app14031098

Academic Editor: Ernesto Limiti

Received: 28 November 2023
Revised: 19 January 2024
Accepted: 24 January 2024
Published: 28 January 2024

1. Introduction

Current fifth-generation (5G) technology is capable, efficient and flexible, but can be further improved. With the densification of cellular networks, where each cell has an identical capacity, covering the same area with smaller cells allows us to support more traffic. As a result, 5G supports higher traffic per cell than fourth-generation (4G) technology; this is also due to higher available bandwidths and more efficient transmission modes that allow us to send more bits per frequency unit. The use of network densification is a key player in 5G, requiring a wide deployment of small cells and thus increasing infrastructure cost and reducing energy efficiency (EE). Reconfigurable intelligent surfaces (RISs) are also capable of increasing throughput and coverage performance with high EE. Therefore, they can potentially be the right replacement for sites with BS as they do not increase the infrastructure cost and increase the EE. Orthogonal frequency division multiplexing

(OFDM), and mMIMO systems [1] are two of several pillars of 5G technology that works in both bands, below 6 GHz and above 24 GHz (mmWave), according to 5G New Radio (5G NR) [2], accommodating more users than the fourth generation. The use of the mMIMO approach allows for 100× higher efficiency without requiring additional base stations (BSs). Non-orthogonal multiple access (NOMA) [3] is used in wideband networks and can accommodate an higher number of users and streams, but fails to achieve a higher EE that is required to meet the challenges and requirements of beyond 5G (B5G) and future generations (6G). Another 5G technology is carrier aggregation, which started in 4G and allows users to be served by carriers from 5G NR and LTE-Advanced at the same time [4]. This requires the terminals' support to work at different frequency bands, namely, sub-6 GHz and beyond 24 GHz. The cloud or centralized radio access network (C-RAN) is another primary component of 5G used to mitigate the effects of users located at cell borders. As networks exponentially grow in size, the cloud alone is not enough, and edge computing is essential. Security is also part of 5G technology, and is deployed on a large scale such as in software-defined networks (SDNs) and network function virtualization (NFV), where software-level components can be attacked [5].

Another use case of 5G is massive Internet of Things (mIoT) or massive machine-type communications (mMTC) supporting 5G IoT use cases with billions of connected IoT devices and sensors. The use case covers both low-data-rate/low-bandwidth IoT devices with infrequent bursts of data requiring long battery life as well as very-high-bandwidth/data-rate IoT devices. These billions of IoT devices represent a real challenge in current 5G wireless networks [6,7]. To support the massive connectivity of IoT devices, powerful and versatile BSs are required close to the data centers. mMIMO has the capability to vastly increase spectral efficiency (SE) and EE. Moreover, mMIMO has the capacity to support the massive connectivity of IoT devices, as has already been shown in the literature [8,9]. In general, a single cell can be used to support IoT networks, such as a smart factory. However, for a smart city scenario, there is a need for a cellular network and a C-RAN. In this article, we assume that the number of IoT devices is greater than the number of service antennas in mMIMO. Orthogonal reference signals (RS) are reused in each sector of a cell with a transmission and reception point (TRP) consisting of a mMIMO. Our objective is to serve as many low-rate IoT devices as possible, given the time and bandwidth of coherence of the channel characteristic of the smart city scenario.

RISs can be synthesized as "intelligent" surfaces comprising a large set of periodic elements that can change the phase (and also the amplitude) of incident waves [10]. RIS may be attached to practically any surface, including walls, furniture, building panels, and clothes. Since RISs have low power consumption and the possibility to be embedded in surrounding objects, these surfaces can be seen as a cost-effective solution for future wireless networks [11]. We extend our previous work in [12], where we presented an iterative algorithm for RIS-empowered systems to accomplish the joint design of the access point precoder and phase-shifts of the RIS elements, considering a multi-stream MIMO-OFDM link. The strategy aimed to maximize the achievable rate in multicarrier point-to-point MIMO communication. The proposed algorithm used the alternating maximization (AM) method to decouple the optimization variables and split the main problem into two simpler ones. The first subproblem was solved using singular value decomposition (SVD) combined with water filling, whereas the second one was addressed with the accelerated proximal gradient (APG) approach. The resulting algorithm was designated an AM-SVD-APG iterative algorithm. The emphasis of this article is joint precoding and RIS optimization and finding the best places to position the RIS for downlink communications.

B5G networks using radio access virtualization strategies, and advanced computational platforms will exploit network densification. The virtual cell concept removes the traditional cell boundary for the end IoT device and provides a consequent reduction in the detrimental "cell-edge experience" for the end IoT device. Traditionally, IoT devices are associated with a cell and, as a consequence, the link performance may degrade as a terminal is located far away from the cell center. In a C-RAN, the network determines which BSs are

to be associated with each IoT device. It seems that the cell is moving with the IoT device in order to provide a cell-center experience throughout the entire network. Each IoT device is served by its preferred set of BSs. The actual serving set for a IoT device may contain one or multiple BSs and the IoT device's data are partially or fully available at some or a small set of potential serving BSs. The BS controller (central processor) will accommodate each IoT device with its preferred set and transmission mode at every communication instance while considering load and channel state information (CSI) knowledge associated with the BS [13].

We will consider a 5G NR system [14–18] using scalable OFDM numerology introducing specific subcarrier spacing (SCS), a transmission time interval (TTI), a cyclic prefix (CP), and the number of slots. Higher numerology indices correspond to larger SCS. The numerology index n depends on various factors (i.e., service requirements, deployment type, carrier frequency, etc.). The introduction of wider SCS is essential for mitigating inter-carrier interference (ICI) and phase noise at millimeter-wave (mmWave) and Terahertz (THz) frequencies. The TTI assumes smaller values ranging from 1 ms to 31.25 µs for numerology 0 and 5, respectively. Moreover, 5G NR was designed to lower interference and increase EE by reducing always-on transmissions, which is a crucial aspect of extending the lifetime of IoT devices; 5G NR ensures forward compatibility, as it is prepared for future 6G evolution in use cases and technologies. At mmWave and THz frequencies, high capacity and extreme data rates are possible, even though higher frequencies introduce limitations in coverage due to increased signal attenuation [19]. The specifications of 5G NR are projected to accommodate dense urban and micro or indoor scenarios, but with the introduction of mmWave and THz, it may be more likely that some part of the signal is blocked by obstacles or severely affected by distance, which causes a substantial decrease in the signal strength, making it hard to compensate for without the use of RIS elements and advanced signal processing [20,21].

The large distance attenuation that takes place in the mmWave and THz bands makes it difficult to achieve large coverage under the limitation of the maximum available terminal or BS transmit power. This phenomenon tends to worsen, especially in systems designed for outdoor environments. Another particular characteristic that is verified at mmWave and THz bands is that the propagation channel tends to be spatially sparse, which results in a lower number of propagation paths. Such challenges can be attenuated with the aid of RISs, since these IoT devices can operate as a centralized beamformer that can increase the channel gains. Moreover, RIS can also create additional propagation paths around major obstacles and enable line-of-sight (LOS) links to distant receivers [22]. In [23], the authors studied a system operating at the THz band using an RIS for an indoor and outdoor scenario that optimizes the phase shifts of the individual elements in order to assist an ultra-massive MIMO (um-MIMO) communication link. Performance results showed that the approach was capable of effectively extending the communication range. The authors in [24], developed an algorithm to calculate the ideal phases for each RIS element in order to maximize the capacity of the transmission. In their study, a multiple-input–multiple-output–OFDM (MIMO-OFDM) link with a frequency-selective fading channel and perfect channel state information was considered.

According to the literature, due to their EE, RISs can be a viable alternative to traditional amplifiers and relays when considering multi-user communication scenarios, as demonstrated by the authors in [25]. The authors in [26] described a system with a single AP that distributes packets to several users. The system is able to improve the performance of both orthogonal multiple access (OMA) and NOMA with the aid of RIS. Although they considered only a single antenna for both transmitter and receiver, it was proved that RIS can enhance both the capacity and rate of the system. Nevertheless, point-to-point communications in MIMO systems aided by RIS are still a challenge. Although some results obtained with system-level evaluations of wireless cellular networks and test bench prototypes exist in the literature [27–30], they all comprise small-scale configurations. Furthermore, the use of RIS-assisted systems combined with MIMO configurations in C-RAN

requires more in-depth research into the optimization process and overall impact. In [31], an RIS-aided cellular network was considered, and an algorithm for joint optimization of active beamforming at the BS and passive beamforming of the RIS was also presented. Their simulation results showed some performance improvements against other existing algorithms. In [32], the authors presented one of the first system-level studies of RIS-aided network deployment, using two frequencies of fifth-generation new radio (5G NR), namely, 3.5 GHz and 28 GHz. While assuming a simplified operation in the far-field region with the RISs configured as anomalous reflectors, they demonstrated through a three-dimensional simulator how RISs can benefit a typical 5G urban network. Additionally, in [33], the authors studied a system-level design with an improved antenna model that analyses the path loss, power, and overall coverage between the transmitter and receiver with the aid of relayed RIS. Their results showed that the impact of the placement of RIS can affect the performance of the system, especially at the edges of the sector cell. Despite the promising results of these initial studies, more research on the integration of RIS in future wireless networks is required before large-scale experimental deployments can become a reality. In fact, at mm-Wave or THz frequencies, the distances between BSs will tend to be short, enabling users to be connected to more than one BS simultaneously.

We adopt the same optimization approach from [12], namely, the joint AM-SVD-APG iterative algorithm applied to the uplink and downlink to effectively enable the implementation of smart radio environments. The use of C-RAN is essential in order to increase the capacity, i.e., the number of active IoT devices in a smart city scenario, and improve the coverage and throughput of other outdoor and indoor scenarios, namely, a stadium with a pitch and an indoor factory. The following is a summary of the article's main contributions:

- We provide a system-level assessment of C-RANs including multiple RISs spread around BSs in three different scenarios at three different frequency bands, namely, 3.6 GHz, 28 GHz and 100 GHz;
- A system-level evaluation for multi-stream MIMO-OFDM links is performed for numerologies 0 and 3 from 5G NR in three 3D scenarios with different parameters, numbers of transmitting/receiving antennas, bandwidths, frequency carriers, numbers of RIS elements, degrees of transmitting power, etc.;
- System-level evaluation demonstrates that C-RAN deployments in all simulated scenarios, including an urban smart city, a stadium with a pitch, and an indoor factory, can achieve significant performance improvements over typical cellular networks without RISs, in terms of both EE and SE.

The article is organized as follows: Section 2 presents the model for the C-RAN system with RIS. Section 3 presents the system-level configuration and scenarios that are considered in the evaluation and also presents and discusses system-level simulation results. The conclusions are outlined in Section 4.

2. System Model

We consider Figure 1 as the basis of our communication system with RIS. It is assumed that the system uses OFDM to cope with frequency-selective fading. In this study, we consider three different scenarios; two of them are outdoor and indoor, and the last one is indoor only. In every scenario, there are surrounding obstacles that can easily block or obstruct communication links. Such a fact presents itself as critical especially in cases where direct LOS is used, or when the signal suffers attenuation losses. LOS and NLOS cases can be assisted with RIS panels. We consider the downlink and uplink of an OFDM-based mMIMO system, where a BS is equipped with N_{tx}/N_{rx} antennas that transmit to N_u users. Between each BS and the users, there are plenty of RIS panels with N_{RIS}-reflecting elements. Each piece of user equipment (UE), which can be an IoT device or a pedestrian, is assumed to have N_{rx}/N_{tx} antennas, wherein that transmission/reception is composed by grouping the subcarriers into N_{prb} physical resource blocks (PRBs), with 12 subcarriers

in each at any given moment. We denote N_s as the total number of streams assigned to the antennas on each subcarrier with modulated symbols to be transmitted/received by the active antennas. In our scenarios, the communication for different users is based on orthogonal multiple access, and we adopt the optimization method that we proposed in [33], which jointly computes the precoder and the phase-shifts of the RIS panels placed in the vicinity of the receiver and transmitter. Such a strategy aims to maximize the achievable rate in multicarrier point-to-point MIMO communication. The adopted algorithm uses the alternating maximization (AM) method to decouple the optimization variables and split the main problem into two simpler ones. The first subproblem is then solved using the singular value decomposition (SVD) combined with water filling, whereas the second one is addressed with the accelerated proximal gradient (APG) approach. We refer to the resulting algorithm as AM-SVD-APG. Table I of [12] summarizes all steps of the proposed joint precoding and RIS optimization algorithm named AM-SVD-APG. This method relies on iteratively applying a gradient-based step followed by proximal mapping.

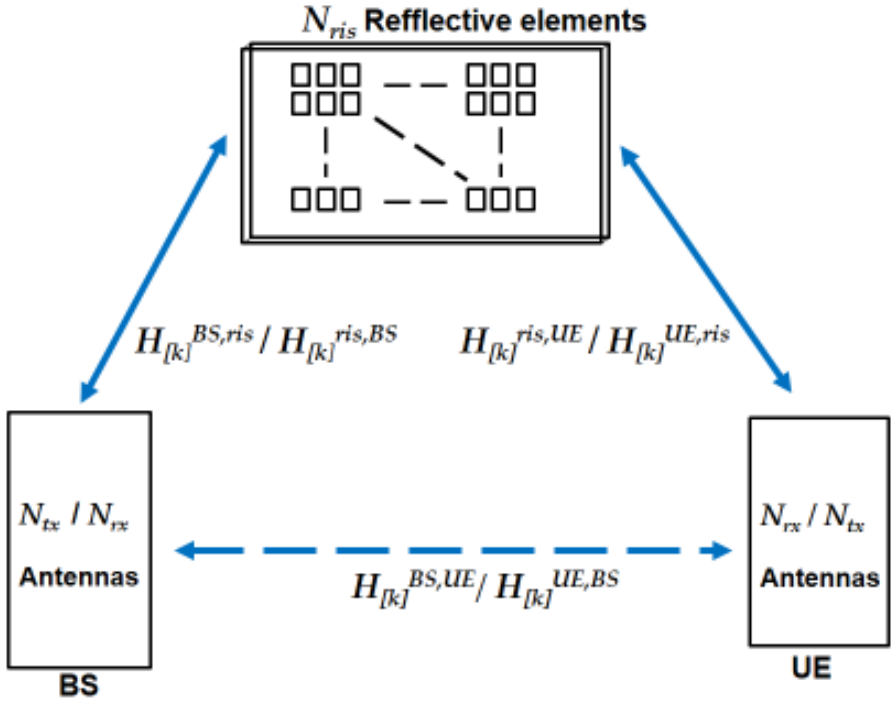

Figure 1. Illustration of a mMIMO communication system aided by RIS, consisting of BS, UE, and RIS with N_{ris}-reflecting elements.

Operators of 5G mobile networks (MNOs) are looking to adopt open, virtualized, C-RAN networks for greater network flexibility and cost savings. MNOs have been moving their networks from physical hardware to virtual and cloud-based software deployments since 4G. This step towards virtualization is well underway for the core network. This goal is also valid for the RAN of 5G and B5G. Cell site antennas have remote radio unit (RRUs) connecting to the central office where the baseband unit (BBU) is localized, with the option of intermediate distributed units with intelligence processing, as shown in Figure 2. The processing power distribution between BBU and RRU depends on the specific use case and scenario. As shown in Figure 2, each transmission and reception point (TRP) is equipped with one uniform planar array (UPA) of antennas per sector.

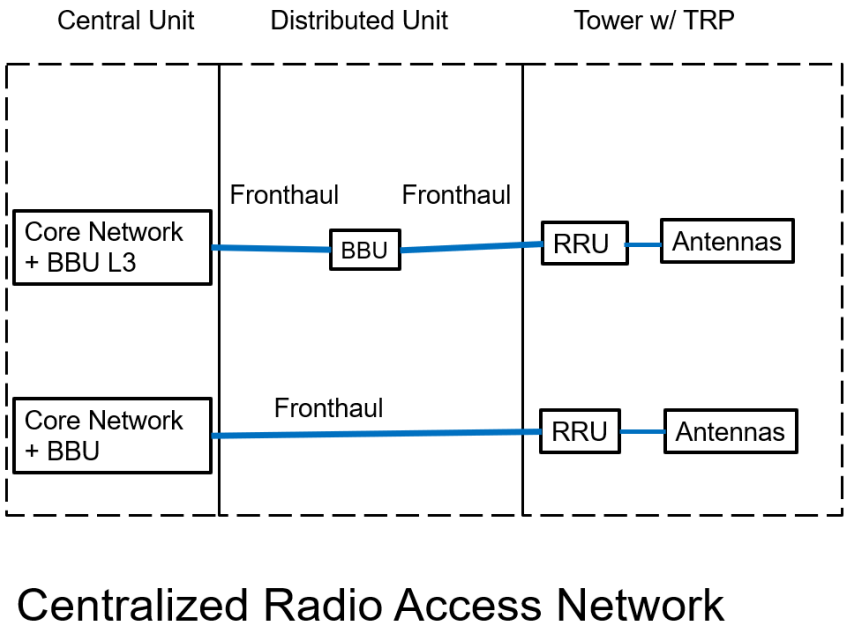

Figure 2. C-RAN illustration.

2.1. Scenarios Based on 5G New Radio 3D Scenarios

There are several 5G test scenarios [14,15]. In this article, we have considered three modified scenarios that are described next and later evaluated using OFDM with mMIMO and RIS communications. For increasing frequency bands, a decrease in the range occurs due to higher power attenuation. We have chosen frequency bands adequate for each scenario. The lower frequency band (sub 6 GHz) with a larger range is adequate for the smart city scenario. The intermediate mmWave with a 28 GHz frequency carrier will be tested for the smart city with RIS and also for the stadium with a pitch scenario. The upper frequency of 100 GHz (THz) with a smaller range will be tested for the indoor factory scenario. While the adoption of BS antenna arrays and RIS panels with a large number of elements (N_{rx}/N_{tx} and N_{ris}) can result in substantial performance improvements in any of the bands, the longer wavelength in the 3.6 GHz band imposes a major physical constraint on the deployment of these large panels. Therefore, it is more feasible to harvest the potential gains associated with the adoption of large antenna arrays and RISs in the 28 GHz and 100 GHz bands, which can help reduce the performance gap relative to the 3.6 GHz case.

The user mobility is selected based on the type of user and the scenario. For IoT devices in the smart city scenario, we have chosen static IoT devices, so the velocity is set as 0 km/h. For the other scenarios, pedestrians have a velocity of 3 km/h, unless they are in the stadium stands, where they are also static.

2.1.1. Smart City

The smart city scenario that we consider is based on a modified section of the urban micro cell with high IoT device densities but with low traffic load per IoT device in city centers and dense urban areas. This scenario is coverage-limited because of the small transmission power of IoT devices. It has transmission and reception points (TRPs), with UPA antennas at a height of 10 m. There are four sites with three TRPs, meaning one per sector. The inter-site distance (ISD) in this scenario is 400 m. The carrier frequency is 3.6 GHz and/or 28 GHz. The bandwidth for both carrier frequencies is 50 MHz. A full buffer model is assumed. At least a total of 2250 active IoT devices are distributed per sector of each cell, with 50% of IoT devices being indoor and the remaining 50% IoT devices being outdoor in the streets, either static or moving at a speed of 3 km/h. The layout of this scenario is illustrated in Figure 3.

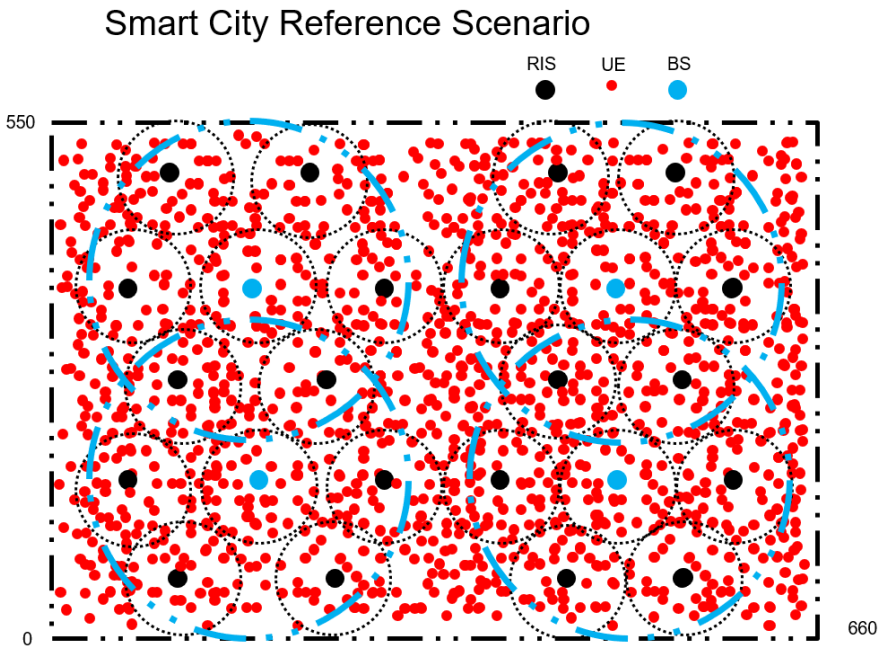

Figure 3. Smart city scenario layout.

2.1.2. Stadium with a Pitch

The stadium with a pitch scenario represents an open-air gathering; it requires a combination of urban micro cells' multi-path fading with small cells and high user densities; there are also higher traffic loads than in the indoor factory scenario, and sparse density clutter with a probability of LOS and NLOS in stadiums with high user densities. This scenario is interference-limited; it has four sites with three TRPs, meaning one per sector. The ISD of this scenario is 108 m. The four sites have a BS antenna height of 25 m. The carrier frequency and bandwidth for this scenario is 28 GHz and 400 MHz. A full buffer traffic model is assumed. A maximum of 3300 users (UEs) are distributed per sector, with 46% of users being in the stadium turf and the remaining 54% being in the stadium stands, which have a height between 2 m and 24 m. The layout of this scenario is illustrated in Figure 4.

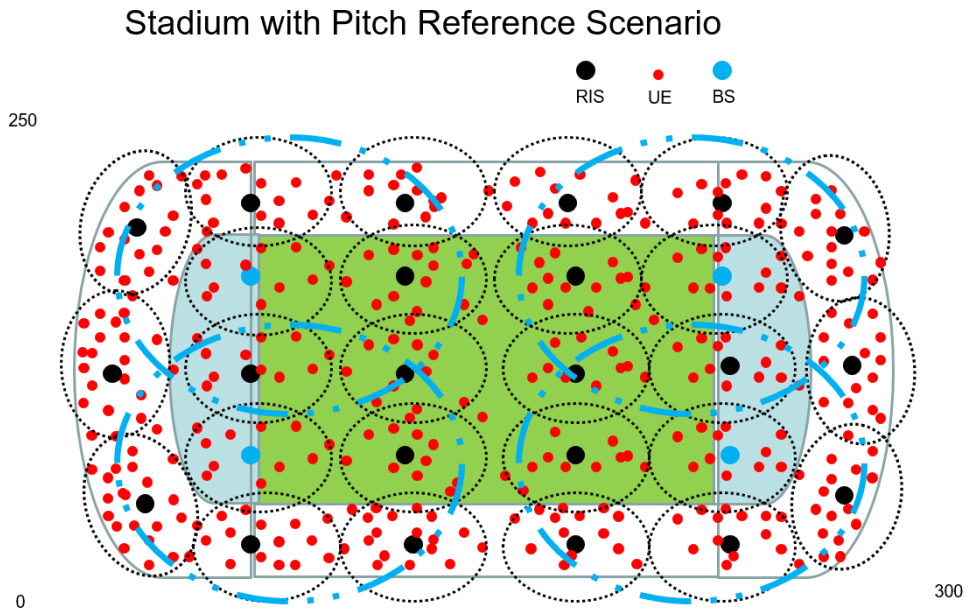

Figure 4. Stadium with pitch scenario layout: microlayer: ISD = 36 m; three TRPs per micro cell.

2.1.3. Indoor Factory

The indoor factory deployment scenario focuses on high user throughput or user density in factories. This scenario represents indoor factories with a total volume of 300 m × 150 m × 10 m. There are two sites with three TRPs, meaning one per sector. The ISD of this scenario is 150 m. In this case, the BS antenna height can be 2 m (low height) or 8 m (high height). It is also an interference-limited scenario. The carrier frequency is 100 GHz (sub THz band). We have chosen only highly clutter-dense factories. The minimum bandwidth is 400 MHz. Variable number of users per cell are distributed uniformly, and the exact number of users depends on the number of physical resource blocks received by each one. Full buffer model is assumed. The layout of this scenario is illustrated in Figure 5.

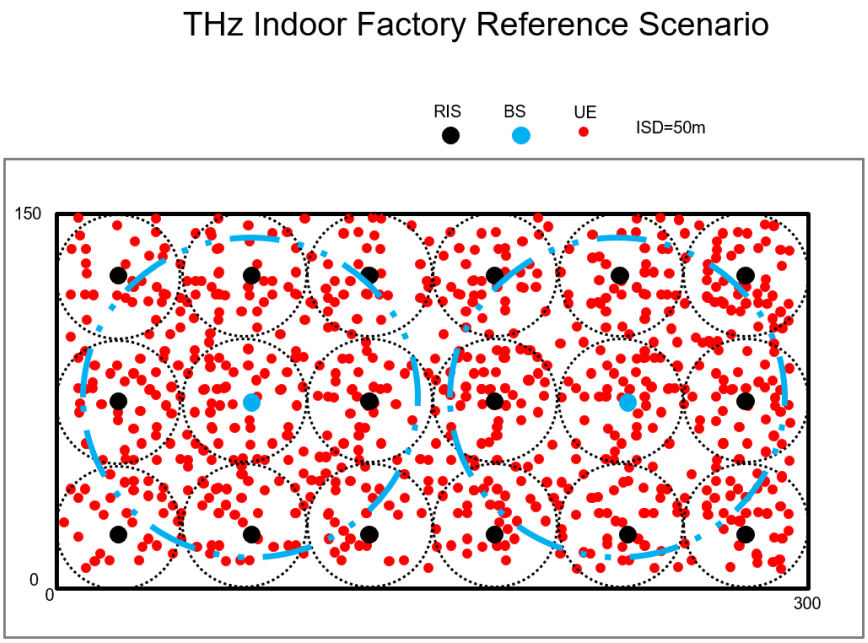

Figure 5. Indoor factory scenario layout.

We have built 3D simulation channel models for the above-mentioned outdoor and indoor scenarios for sub-6 GHz, mmWave, and THz frequencies. All the details about 3D simulation channel models can be found in [15]. For sub-6 GHz frequencies, up to a moderate number of antennas can be activated (i.e., 64). In mmWave frequency bands, the transmission is characterized by a considerable signal attenuation that limits the network coverage. To overcome this limitation, one of the key features is the adoption of a large number of multi-antenna elements having a given aperture to increase the transmission/reception capability of mMIMO and beamforming. Since managing transmissions in mmWave frequency bands is complicated, the beam needs to be optimized and adjusted each time, taking into account the conditions of the receiver and the RIS. However, for direct links between BS and users (or IoT devices) without the involvement of RIS, the correspondence between the directions of the transmitter and receiver-side beams is performed by identifying the most suitable beam pair for both downlink and uplink.

3. System-Level Configuration

In this section, we present the setup adopted for the C-RAN system-level assessment, detailing the target scenarios that we will evaluate. In the C-RAN, the static clustering technique partitions the network into three adjacent TRP sets where each user is served by at least one TRP, while the others perform inter-user interference. For the C-RAN with a cluster size of 1, we have a traditional cellular system. For instance, with cluster size 3, the network is partitioned into three adjacent TRP sets where each user is served by three adjacent TRPs. The inter-user interference only comes from the other clusters. The

considered scenarios are almost all based on modified 3GPP environments as specified in the previous section: the smart city environment, which corresponds to a modified urban micro outdoor/indoor environment; the stadium with pitch, which has no correspondence to any 3GPP environment but corresponds to an open-air gathering environment; and the indoor factory, which is based on the reference scenario of 3GPP, with the same name for an indoor factory environment area (see Figures 3–5).

In our study, the operating frequency varied depending on the scenario. The bandwidth was also variable depending on the 5G NR numerology chosen for the scenario. The bandwidth was B = 50 MHz for numerology 0 and B = 0.4 GHz for numerology 3. In all scenarios, the IoT devices or terminals were uniformly placed within a minimum distance of 1 m around their respective BSs and RIS panels. The red dots on the previous figures illustrating the scenarios represent the IoT devices or users. The IoT devices or users are randomly and uniformly placed in each scenario at a given distance and angle from the BSs or from the associated RIS panel. There is a probability of having LOS and NLOS links depending on the distance d. In the case of the NLOS links, there is fading due to multipaths following a Rayleigh distribution with shadowing, according to a lognormal distribution. All parameters and equations can be found in [15]. For each scenario, the probability of LOS (P_{LOS}) can be calculated as follows:

Smart City Scenario

$$\begin{cases} P_{LOS} = 1, d < 18 \\ P_{LOS} = (18/d + \exp(-d/36) \times (1 - 18/d)), d > 18 \end{cases} \quad (1)$$

Stadium w/Pitch Scenario

$$\begin{cases} k_{sub} = 44.8 \times ((h_{BS} - h_{UT})/(22.5 - h_{UT})), h_{BS} = 25 \\ P_{LOS} = \exp(-(d/k_{sub})) \end{cases} \quad (2)$$

Indoor Factory Scenario

$$\begin{cases} k_{sub} = 2.2, h_{BS} = 2 \\ k_{sub} = 2.2 \times ((h_{BS} - h_{UT})/(6 - h_{UT})), h_{BS} = 8 \\ P_{LOS} = \exp(-(d/k_{sub})) \end{cases} \quad (3)$$

where h_{BS} and h_{UT} are the BS and terminal antenna heights.

In all scenarios, we first evaluate the case where only BSs are active, i.e., RIS are not active. In this case, the coverage area of the BSs must include almost the whole scenario area. Large blue circles are illustrating this situation for every scenario.

For the smart city scenario, one IoT device can be connected to each corresponding RIS panel at height of 10 m, with a total of 20 RISs and 4 BSs deployed. There are five RISs inside each BS coverage area, as represented in Figure 3. For the stadium with pitch scenario, up to three users can also be connected to each corresponding RIS panel at a height of 10 m, with a total of 22 RISs and 4 BSs deployed. There are an average of 5.5 RISs inside each BS coverage area, as represented in Figure 4. For the indoor factory scenario, one user can be connected to each corresponding RIS panel at a height of 2 or 8 m, with a total of 16 RISs and 2 BSs deployed. There are eight RISs inside each BS coverage area, as represented in Figure 5.

The total power transmitted by each BS or IoT device depends on the scenario and the frequency carrier. At 100 GHz, the power was set to 30 mW (14.8 dBm) for the indoor factory, whereas 3.16 W (35 dBm) or 250 mW (24 dBm) were transmitted from each BS at 28 GHz, in the case of the stadium. For the smart city scenario, the power transmitted by IoT devices was set as 10 mW (10 dBm) both for 3.6 GHz and 28 GHz. Two types of links are considered, namely, a direct link between BS and IoT devices or users and an indirect link through the RIS. For all scenarios, because of the C-RAN, there are always double-links, where IoT devices or users are served simultaneously by an RIS and a BS. The noise power is N_0 = −85 dBm for the bandwidth B = 0.4 GHz and N_0 = −94 dBm for the bandwidth

B = 50 MHz. The receiver noise figure F = 3 dB. The spacing between each element of the RIS panel is d_{RIS} = $\lambda/2$ = 42 mm (3.6 GHz), d_{RIS} = $\lambda/2$ = 5.4 mm (28 GHz), and d_{RIS} = 1.5 mm (100 GHz), resulting, respectively, in areas of A = 1764 mm^2, A = 29.16 mm^2, and A = 2.25 mm^2 per element. The gains of the individual antenna elements of the arrays are 0 dBi for both the transmitter and receiver.

Next, we present the parameters considered for these scenarios in Tables 1–3.

Table 1. Parameters of the smart city scenario.

Parameters		Smart City @ 3.6	Smart City @ 28
Area (m^2)		660 × 550 m^2	660 × 550 m^2
Carrier frequency		3.6 GHz	28 GHz
Cell range	w/o RIS	134 m	134 m
	w/ RIS	100 m	100 m
IoT device mobility		0 km/h	0 km/h
IoT device distribution (horizontal)		Uniform	Uniform
Maximum active IoT devices		Up to 19,800	Up to 19,800
Transmission power		10 dBm	10 dBm
IoT devices' antenna gains		0 dBi	0 dBi
Area of RIS elements		1764 mm^2	29.16 mm^2

Table 2. Parameters of the stadium with pitch scenario.

Parameters		Stadium Stands	Stadium Turf
Area (m^2)		168 × 126 m^2	144 × 108 m^2
Carrier frequency		28 GHz	28 GHz
Cell range	w/o RIS	57 m	57 m
	w/RIS	34 m	34 m
User mobility		0 km/h	3 km/h
User distribution (horizontal)		Uniform	Uniform
Maximum UEs attached		Up to 20,923	Up to 18,277
Transmission power		35 dBm & 24 dBm	35 dBm & 24 dBm
BS antenna gains		0 dBi	0 dBi
Area of RIS elements		29.16 mm^2	29.16 mm^2

Table 3. Parameters of the indoor factory scenario.

Parameters		Factory w/Low BS	Factory w/High BS
Area (m^2)		300 × 150 m^2	300 × 150 m^2
Carrier frequency		100 GHz	100 GHz
Cell range	w/o RIS	70 m	70 m
	w/RIS	50 m	50 m
User mobility		3 km/h	3 km/h
User distribution (horizontal)		Uniform	Uniform
Maximum UEs attached		Up to 19,800	Up to 19,800
Transmission Power		14.8 dBm	14.8 dBm
BS antenna gains		0 dBi	0 dBi
Area of RIS elements		2.25 mm^2	2.25 mm^2

3.1. Link-Level Simulations

The performance of the adopted scheme, namely, the joint design of the precoder and phase-shifts of the RIS elements, is assessed considering a MIMO–OFDM link, and compared against other MIMO–OFDM systems. Monte Carlo simulations were run according to the system model presented previously.

Figure 6 shows the BER performance versus the distance between the transmitter and the receiver. The distance between the Tx—Transmitter and the Rx—receiver is presented in the x axis in Figure 6. For this comparison, we use a transmitted power of P_{user} = 10

dBm. We observe curves for five different configurations. The parameters used are N_{tx} = 64, N_s = 3, N_{rx} = 16, N_{ris} = 144 or 576 elements, and N_c = 1. Curves with the proposed AM-SVD-APG algorithm are presented and assume the existence of direct and indirect links between the transmitter and receiver. BER values should decrease along with the reduction in the distance between transmitter and receiver. When this distance is increased, the opposite occurs and there is a distance beyond which the received signal strength becomes low to the point it results in error rates above 0.001. We can check that in Figure 6, BER values are already greater than 0.001 for a distance of 20 m in the case of the curve without RIS, where we are assuming an NLOS link with high attenuation loss between Tx-Rx. When RISs are adopted, it can be seen that the curves improve and the distances where the BER becomes higher than 0.001 increase, reaching 70 m for the case of an RIS with 576 elements combined with the AM-SVD algorithm. To compare with our algorithm, we include results obtained with the APG algorithm from [23]. It can be observed that our scheme clearly outperforms APG.

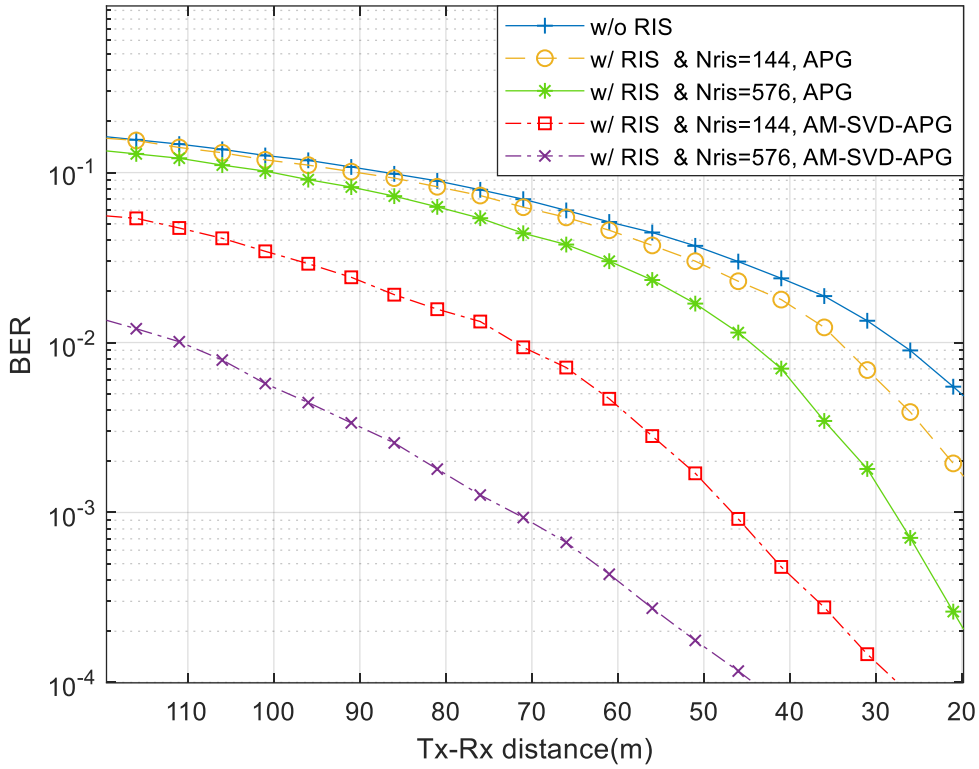

Figure 6. BER versus distance for a scenario with fc = 28 GHz, N_{tx} = 64, N_s = 3, N_{rx} = 16, N_{ris} = 144 or 576 elements with N_c = 1.

3.2. System-Level Simulations

The signal-to-noise ratio (SNR) in dB considered in the system-level simulations is obtained from $SNR = (E_s/N_0) + 10\ log(Rs/B)$ dB, where Rs is the total transmitted symbol rate per antenna and user, B is the total bandwidth (we considered 50 MHz at 3.6 GHz and 28 GHz for the smart city with numerology 0, and 400 MHz at 28 GHz and 100 GHz for the other scenarios with numerology 3), and E_s/N_0 is the ratio of symbol energy to noise spectral density in dB. Values of E_s/N_0 are obtained from the link-level BER results. In this work, we only considered QPSK modulated symbols. The frame structure of 5G NR has both a frequency division duplex (FDD), used in the paired spectrum, and a time division duplex (TDD), used for the unpaired spectrum. We chose TDD in this work for all scenarios.

The subcarrier spacing, transmission time interval, cyclic prefix (CP), and the number of symbols per slot are all defined by the proposed 5G NR scalable OFDM numerology [15].

Our scenarios were simulated considering numerologies 0 and 3. Numerology 0 (4G) was chosen for smart city scenario because the most important key performance indicator (KPI) is the coverage of IoT devices, not their throughput, and numerology 3 for the stadium with pitch and indoor factory scenarios, in mmWave and THz bands, respectively.

For the smart city scenario, we considered different UPA antenna arrays with N_{rx} = 144, 256, and up to 576 elements on the receiver side (BS). For the IoT device (on the transmitter side), N_{tx} = 1, N_s = 1 and N_c = 1. For numerology 0, Δf = 15 KHz, and every PRB has 12 carriers (B_{prb} = 180 KHz) with 14 symbols per subframe duration Ts = 1 ms, with 168 (12 × 14) subcarriers. In real cellular networks with massive MIMO, there is a coherence interval where channel information does not change much, and pilot reference symbols must be retransmitted. The coherence interval is

$$\tau_c = T_c \times B_c \tag{4}$$

where coherence time T_c = 50 ms is well fitted for nomadic and static low-power IoT devices [34], and B_c = 1.697 MHz (9.42857 × 180 KHz) is adequate for an urban city scenario such as a smart city. In τ_c, the maximum number of subcarriers is N_{sc} = 79,200 (168 × 50 × 9.42857). Half of the coherence interval can be used for uplink data transmission, and the remaining half of the coherence interval can be used for downlink transmission. We need orthogonal reference pilots in uplink that must be subtracted from uplink data symbols. For uplink data and reference pilots, we must have $N_{sc}/4$ = 79,200/4 = 19,800 subcarriers. Assuming that we divide 19,800 into twelve groups (scenario has 4 BS × 3 sectors), then we obtain 19,800/12 = 1650 subcarriers, one for each IoT device transmitting in each sector at the same time without any intra-cell interference. Table 4 presents the additional simulation parameters of the smart city scenario. In real situations, the number of active IoT devices per sector can be much higher because of the sleeping time of IoT devices. Sensors do not need to transmit packets every 1 ms.

Table 4. Additional simulation parameters for the smart city scenario.

Parameter	Value
Coherence time Tc	50 ms
Coherence band Bc	1.697 MHz
Maximum time Tp	12.5 ms
Maximum N_{sc}	79,200
Max. active IoT devices $N_{sc}/4$	19,800
Number of sectors	12
Number of IoT devices/sector	1650

For the smart city scenario, we consider only the uplink, wherein IoT devices are transmitting to BS and RIS at the same time. Uplink power control is appropriately applied so that the received powers are the same for almost all IoT devices. However, data sent from IoT devices that are too far from the receivers, i.e., BSs and/or RISs, might not be well received. There is a minimum received power that must be above the receiver sensitivity so that packets are correctly received. We take as a reference the BER $\leq 5 \times 10^{-4}$ to decide which packets are received without bit error. For numerology 0 of 5G NR, Δf = 15 KHz and 168 subcarriers are being transmitted in every PRB during 1 ms. The minimum throughput of each IoT device is 2 Kbps, assuming transmission in one carrier with QPSK symbols, and the minimum spectral efficiency per IoT device is ε_u = 2/15 bps/Hz. There is a theoretical equation for the maximum throughput, assuming perfect power control and a single cell with no inter-cell interference [9], which is

$$Th_{max} = 0.5 \times B \times (1 - \tau_p) \times \log_2(1 + SINR) \tag{5}$$

where τ_p is fraction of time for pilot symbols' transmission and B is the total bandwidth. SINR is the signal to interference plus noise ratio.

In Figure 7, the throughput performance versus number of users is shown for different number of antennas at BS in each sector of the scenario, and for different frequency carriers. The throughput curves in Figure 7 were obtained with a maximum transmitted power of 10 mW. The settings are described in Table 1. In this scenario, we used $N_s = 1$, $N_c = 1$, $N_{tx} = 1$, and $N_{rx} = 144$, 256 or 576 antennas. As expected, the frequency carrier of 3.6 GHz provides the highest throughput compared to 28 GHz due to its lower path attenuation. Increasing N_{rx} provides higher throughput independently of the frequency carrier. Increasing the number of UPA antennas allows us to more efficiently serve more IoT devices at the same time. For almost all curves, as N_{rx} increases, the throughput increases up to a certain point, and then it decreases. The decrease in throughput after a certain N_u depends on N_{rx}. Increasing N_u above N_{rx}, at sector level, increases intra-cell and inter-cell interferences, thus decreasing the throughput. In addition, there are higher number of IoT devices at the border of the cells with SINR below the reference to avoid errors in packet. Due to the C-RAN operation mode, almost no reference pilot symbol contamination occurs. For 3.6 GHz, the maximum simulated spectral efficiency occurs for N_u = 19,800 and N_{rx} = 576, corresponding to $\varepsilon = 508/24.75 = 20.53$ bps/Hz, where 508 Mbps is the aggregate throughput of 19,800 IoT devices and B = 24.75 MHz is the occupied bandwidth. The theoretical maximum spectral efficiency is $\varepsilon_{\max} = 554/24.75 = 22.40$ bps/Hz.

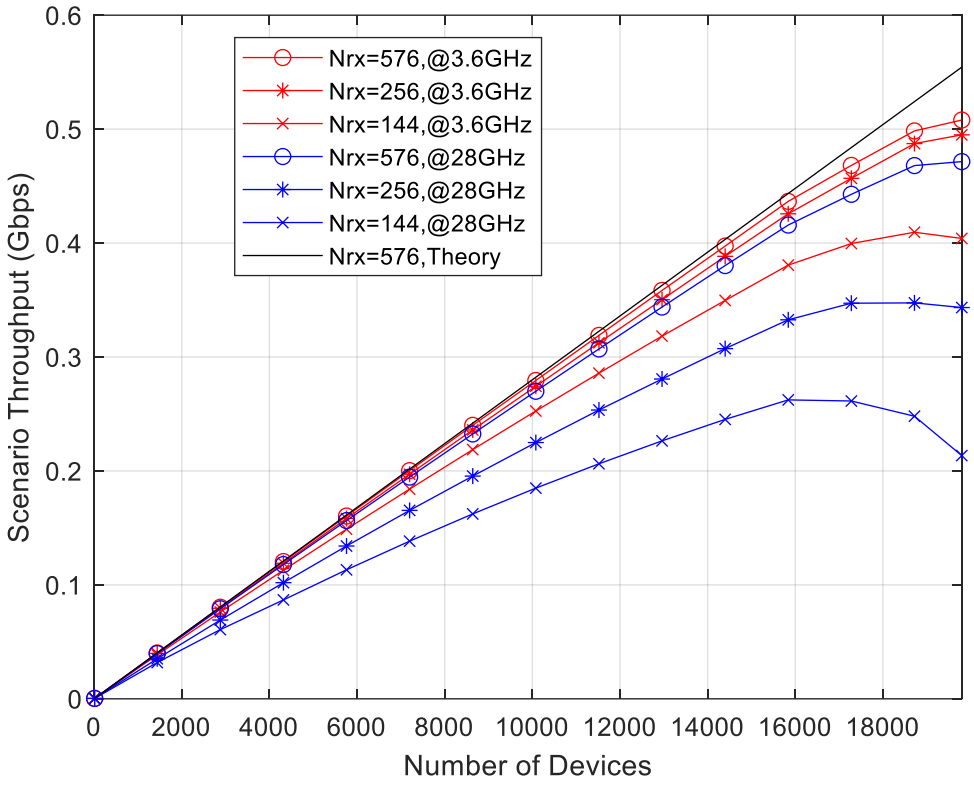

Figure 7. Throughput vs. number of IoT devices for a smart city scenario with N_{tx} = 1 and P_{tx} = 10 dBm, for carrier frequencies of 3.6 GHz and 28 GHz.

In Figure 8, the throughput performance versus N_u is shown for a different number of antennas at BS in each sector and a carrier frequency of 28 GHz, both without and with RIS panels (N_{ris} = 576). We compare four standard communication curves without any RIS, only with BSs and IoT devices, with three curves with RISs panels spread around the scenario. The former curves consist only of direct links between the IoT devices and the receivers. The other cases consist of a combination of direct link connections and RIS-aided connections. They are represented as a percentage of IoT devices that are transmitting signals to BS plus the percentage of IoT devices also with RIS connections, namely %BS + %RIS. For example, 100%BS + 0%RIS means that all IoT devices are attached to the BSs,

whereas 89%BS + 11%RIS represents 89% of spread-out IoT devices linked to nearest BS, and the 11% remaining IoT devices are linked to nearest RISs. C-RAN processes data received from the two best links involving each IoT device. For example, as shown in Figure 7, depending on N_{rx}, the throughput increases up to a certain point, and then it decreases. The decrease in throughput after a certain N_u depends on N_{rx}. At sector level, increasing N_u above N_{rx} increases intra-cell and inter-cell interferences, thus decreasing the throughput. As expected, the introduction of RIS panels at cell borders provides higher throughput compared to BS-only connections. As expected, increasing the number of receiving UPA antennas results in higher throughput due to their higher multiple-access capability. The throughput gain introduced by RIS panels with N_{ris} = 576 increases with the decreasing number of UPA antennas N_{rx} = 576, 256 and 144. The gain is more noticeable for increasing N_u, because more users become close to where RIS panels are localized at the cell borders. Only for 28 GHz have we considered a UPA with N_{rx} = 1024 antennas because of its size. As expected, the maximum throughput is achieved for N_{rx} = 1024 due to its higher multiple-access capability.

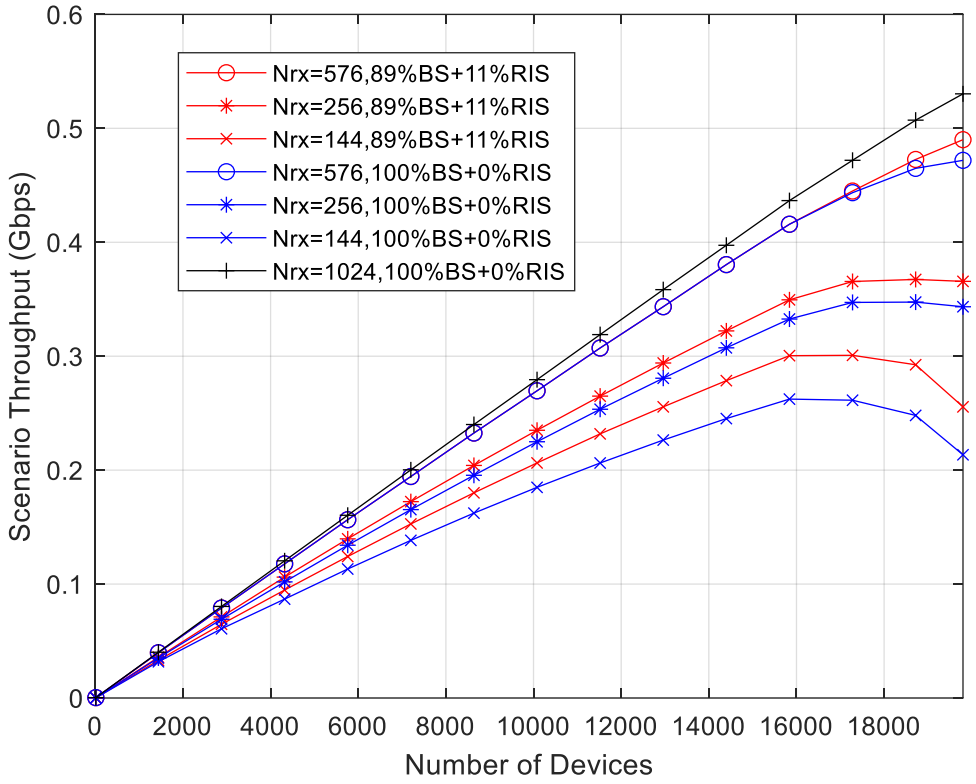

Figure 8. Throughput vs. number of IoT devices for the smart city scenario with N_{tx} = 1 and P_{tx} = 10 dBm, for a carrier frequency of 28 GHz, N_{ris} = 576.

Figure 9 presents the coverage versus transmitted power for N_u = 19,800 with the same conditions as Figure 8. The comparison between Figures 8 and 9 shows that there is a direct correspondence between the throughput performance and the associated coverage. For the maximum transmitted power of 10 mW, the smallest coverage of 44% is achieved by the curve 100%BS + 0%RIS, N_{rx} = 144, whereas the highest coverage is 93% which is obtained by the curve 100%BS + 0%RIS, N_{rx} = 1024. Thus, the maximum coverage gain is 111%. The next highest coverage of 90% corresponds to the curve 89%BS + 11%RIS, N_{rx} = 576 and represents a coverage gain of 104% that includes a reduction in the number of antennas but the introduction of RIS. Still, the main contribution to the coverage gain is due to the number of antennas, which is 97%.

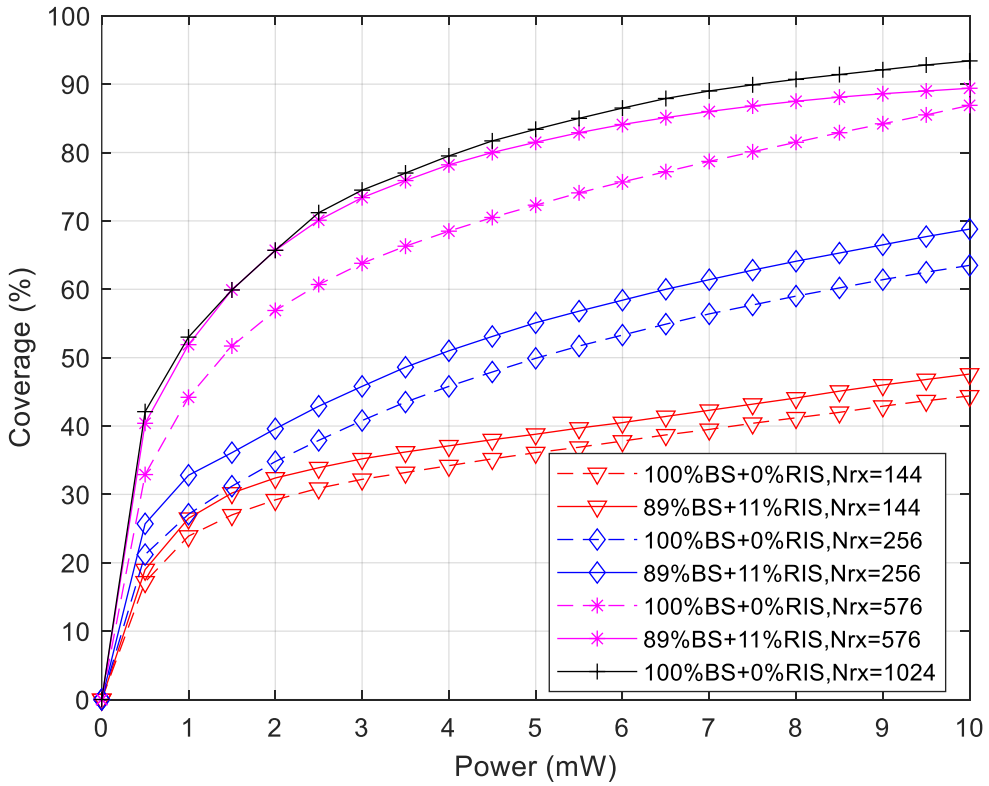

Figure 9. Coverage vs. transmitted power for the smart city scenario with a carrier frequency of 28 GHz with N_u = 19800, N_{ris} = 576.

Next, we tested the stadium with pitch scenario with different parameters. For this purpose, we adopted a higher number of subcarriers N_c combined with more spatial streams and larger transmit powers. The numerology of 5G NR is 3, with Δf = 120 KHz; the bandwidth is 400 MHz, and 112 symbols are transmitted every millisecond. The maximum number of subcarriers is 3300. In this scenario, the main KPI is throughput associated with the number of connections per unit of area. In all simulations in the stadium, the transmitter-side BS has N_{tx} = 64, whereas the receiver-side user has the same number of antennas, namely, N_{rx} = 16. Different numbers of transmitted symbols per subcarrier were considered in the simulations: N_s = 2 and N_s = 3. The number of OFDM subcarriers (N_c) used in the evaluations is variable, namely, N_c = 12, 60, 120, 132, 216 or 240. All these numbers are multiples of 12, which correspond to the number of subcarriers of a PRB in 5G NR.

Users are placed uniformly around TRPs localized close to the four corners of the stadium turf. Some 46% of users are on turf, while the remaining 54% are sitting in the stadium stands (see Figure 4 and Table 2). The configuration with 100%BS + 0%RIS has 4 BSs and 12 sectors and matches a typical cellular system. In this case, users are uniformly distributed within a radius of 57 m (see Table 2). On the other hand, when simulating cases with BSs and RISs operating simultaneously, users that are connected to BSs will be uniformly distributed within a circle with a radius of 34 m. RIS panels are uniformly distributed inside the scenario, and users served by RISs are distributed uniformly within a radius of 17 m.

In Figure 10, the throughput performance versus the number of users in the stadium scenario is shown. The throughput curves of Figure 10 were obtained with a maximum transmitted power of 250 mW. The total number of users in each sector is determined by the total number of subcarriers divided by the required number of subcarriers to achieve the specific bit rate. For Bt = 400 MHz and numerology 3, there are a total of 3300 subcarriers for data transmission. We kept the maximum number of subcarriers at 3300 to avoid intra-cell

(sector) interference. When we consider 11 PRBs per user, i.e., N_c = 132, the maximum number of users per sector is 3300/132 = 25. When RISs are inserted in the border of the sector, a proportion of the 25 users are assigned to them. In this scenario, there are 12 sectors and four BSs, each one with 3 sectors. The total number of served users at the same time in the Stadium is 25 × 12 = 300. Two different RIS sizes appear, since each RIS panel is divided into sub-panels when serving more than one user. We have N_{RIS} = 192 and 576 elements. When users are served with a direct link only from BS (100%BS + 0%RIS), we have a total average throughput of approximately 48 Gbps for 300 users (represented as a red line). In the stadium, there are 22 × 3 = 66 RIS panels and 4 × 3 = 12 TRPs. Considering the black and blue lines, when users at cell borders start to be served by RIS panels, 66 users from 300 (i.e., 66/300 = 0.22) must be subtracted, resulting in 300 – 66 = 234 users (i.e., 234/300 = 0.78) who are served by 12 TRPs, 78%BS + 22%RIS. For the pink and green lines, when 66 × 3 = 198 users are served by RIS 198/300 = 0.66, the remaining 300 – 198 = 102 users (i.e., 102/300 = 0.34) are served by TRPs, 34%BS + 66%RIS. We observe that the throughput gain of curves with N_s = 3 compared to N_s = 2, is 1.5. There is no difference in throughput between users served by an RIS (0%BS) and users served by a BS (0%RIS). If more users are served by RIS panels (66%RIS), there is a throughput decrease compared to curves with fewer users (22%RIS), which is only noticeable for N_s = 3 (curves black and pink). For N_s = 2, there is no decrease in throughput when more users are served by the same RIS panel (curves blue and green). Note that in all curves, there is no decrease in throughput for increasing N_u, because C-RAN operation combines transmitted signal power to RIS and BS, decreasing substantially inter-cell interference. We are also assuming perfect CSI in link-level results, and there is no intra-cell interference, as explained above.

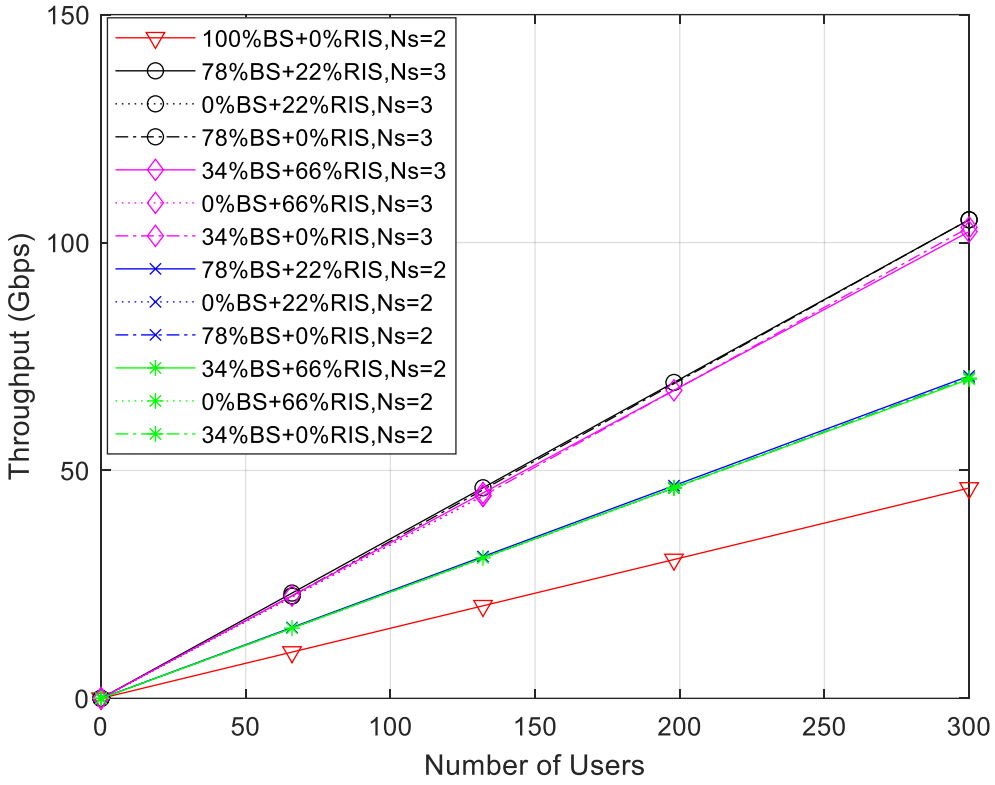

Figure 10. Throughput vs. number of users for the stadium with pitch scenario, with 11 PRB, N_{tx} = 64, N_{rx} = 16, two different N_{ris} = 576 (22%RIS), N_{ris} = 192 (66%RIS), and P_{tx} = 24 dBm.

In Figure 11, the throughput performance versus N_u is shown for the stadium scenario, with two different maximum transmitted powers from BSs. Low-power BSs (LPBSs) transmit 250 mW, and high-power BSs (HPBS) transmit 3.16 W. We keep the maximum number of subcarriers of 3300 to avoid intra-sector interference. We assign 10 PRBs per user,

i.e., N_c = 120, and 20 PRBs per user, N_c = 240. With 10 PRBs to each user, 3300/120 = 27.5 is the number of users per sector. The total number of served users in the stadium at the same time is 27.5 × 12 = 330. With 20 PRBs to each user, there are 3300/240 = 13.75 users per sector. The total number of users served at the same time in the stadium is 13.75 × 12 = 165. When users are exclusively served by the TRPs of BSs with direct links, i.e., 100%BS + 0%RIS, we have a total throughput of approximately 53 Gbps for 330 users (the pink line), and a total throughput of 48 Gbps for 165 users (the red line). Considering the case of 10 PRBs (blue lines), when 66 users at cell borders are served by an RIS (i.e., 66/330 = 0.20), the remaining 330 – 66 = 264 users are served by TRPs, (i.e., 264/330 = 0.80), 80%BS + 20%RIS,10RB. When 66 × 2 = 132 users are served by an RIS (i.e., 132/330 = 0.40), the remaining 60% users are served by TRP 60%BS + 40%RIS,10RB. Assigning 20 PRBs per user (black lines), when 66 users at cell borders are served by an RIS (i.e., 66/165 = 0.40), 165 – 66 = 99 users are served by TRPs, 99/165 = 0.60, 60%BS + 40%RIS,20RB. When 66 × 2 = 132 users are served by an RIS (i.e., 132/165 = 0.80), the remaining 165 – 132 = 33 users (i.e., 33/132 = 0.20) are served by TRP 20%BS + 80%RIS,20RB. We observed only a very slight decrease in the throughput results when increasing the number of users served by every RIS panel from one to two. There is almost no difference in achieved throughput between HPBS and LPBS. There is a slightly higher throughput for LPBS that is more noticeable for 20RBs. Throughput gains are between 97% for 10RB and 110% for 20RB.

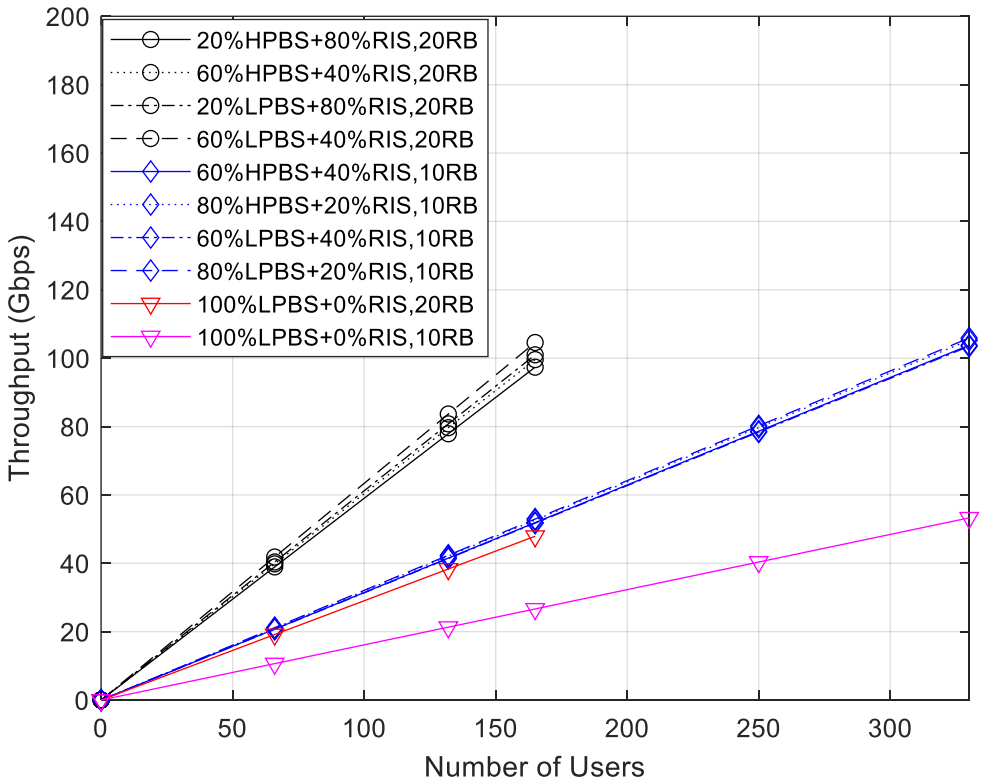

Figure 11. Throughput vs. number of users for the stadium with pitch scenario for two different number of resource blocks: LPBS with BS Power 24 dBm, and HPBS with 35 dBm, N_s = 3, N_{tx} = 64, N_{rx} = 16, N_{ris} = 576 and N_{ris} = 288.

Figure 12 illustrates the average coverage versus transmitted power for both N_c = 120 (10 PRB) and N_c = 240 (20 PRB), corresponding to the throughput performance presented in Figure 11, considering only HPBS, with a maximum transmitted power of 3.16 W (35 dBm). The comparison between Figures 11 and 12 indicates that there is a direct correspondence between the throughput performance of Figure 11 and the associated coverage of Figure 12. However, in terms of coverage, the differences are more noticeable than with throughput. It is noticeable that for the maximum transmitted power, the highest coverage of 99.4% is

achieved by the curve 80%BS + 20%RIS,10RB followed by the curve 60%BS + 40%RIS,10RB. Next follow the curves 60%BS + 40%RIS,20RB and 20%BS + 80%RIS,20RB. It is obvious that when the number of PRBs per user doubles, the coverage decreases. It is also noticeable that doubling the number of users served by RIS panels also decreases the coverage. The lowest coverage values correspond to no RIS panels being activated, i.e., 100%BS + 0%RIS, 10RB and finally, 100%BS + 0%RIS, 20RB, with a coverage of 45.4%. The coverage gain compared to the highest coverage value with 20RB is 111% and is 98% for 10RB.

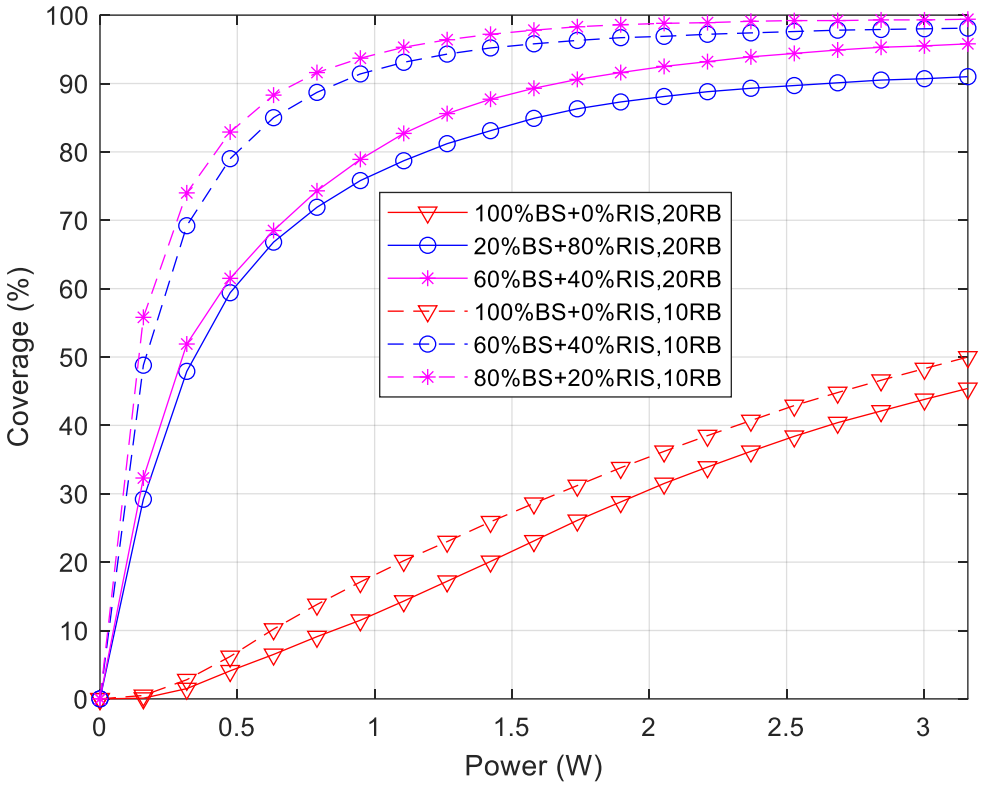

Figure 12. Coverage vs. transmit power for the stadium with pitch scenario for two different number of resource blocks: HPBS transmit power (35 dBm), N_{tx} = 64, N_{rx} = 16, N_{ris} = 576.

In Figure 13, we again consider the stadium scenario, presenting the aggregate throughput for each sector and considering the maximum transmit power of 24 dBm versus the number of PRBs per user. The maximum number of subcarriers is set as 3300 per sector, independently of the number of PRBs per user. We evaluate the sector throughput only for a specific number of PRBs, namely, 1 PRB, 5 PRBs, 10 PRBs, 15 PRBs and 20 PRBs. Assigning 1 PRB per user corresponds to N_c = 12, 5 PRBs per user corresponds to N_c = 60, 10 PRBs per user corresponds to N_c = 120, 15 PRBs per user corresponds to N_c = 180, and finally, 20 PRBs per user requires N_c = 240 subcarriers. The number of users per sector when each user has 1 PRB is 3300/12 = 275. In total, there are 12 sectors in the stadium; thus, there are a total of 3300 active users. For the case in which every active user has 20 PRBs, there are 3300/240 = 13.75 users per sector and the total of active users in the stadium is 165. We observe in Figure 13 that for the curve BS (100%BS + 0%RIS), there is a maximum throughput for 1 PRB, which is the same for the curve BS + RIS. For 5 PRBs and 10 PRBs per user, there is a clear linear decrease in throughput in the red curve (BS) compared to black curve (BS + RIS). The decrease in throughput continues with 15 PRBs and 20 PRBs, but in a slower way. The curve of BS + RIS has almost the same aggregate throughput per sector; however, we noticed a very slight decrease with the increasing number of PRBs. When users are transmitting a higher number of PRBs, the size of packets transmitted is higher and more likely to suffer deep fading. In this case, the link diversity of RIS + BS provided by the C-RAN is able to cope with the expected decrease in throughput.

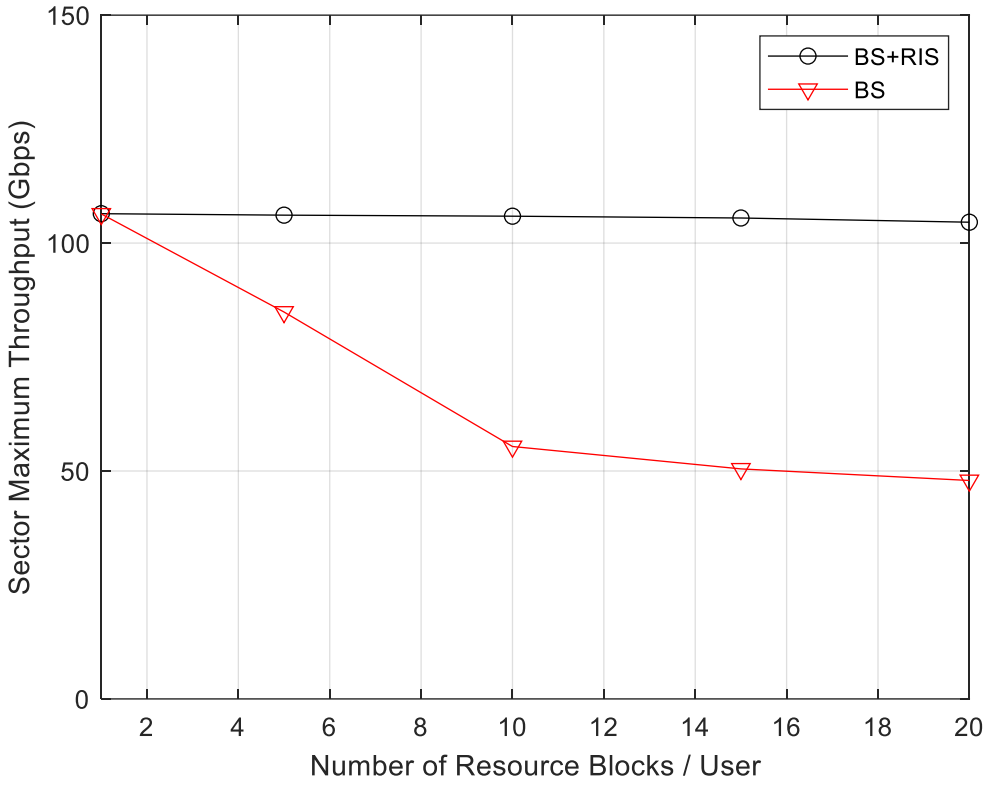

Figure 13. Throughput vs. number of resource blocks for the stadium scenario in the maximum load sector: N_s = 3, N_{tx} = 64, N_{rx} = 16, N_{ris} = 576. LPBS transmit power (24 dBm).

The third evaluated scenario is the indoor factory, which is the only one with a higher frequency band at sub-THz. The system operates at 100 GHz, which, due to its shorter wavelength, allows us to work with more elements at the RIS, i.e., N_{RIS} = 576 up to 2304. The maximum transmit power of BS is 30 mW (14.8 dBm). Users are placed uniformly around two sites with TRPs equipped with UPA antennas per sector, localized 75 m close to the walls of the indoor factory (see Figure 5 and Table 3). We considered there to be a high clutter density inside the Factory, with both low BS antenna height and high BS antenna height. For this scenario, we keep the 5G NR numerology at 3, with Δf = 120 KHz, a bandwidth of 400 MHz, and 112 symbols transmitted in every millisecond, just as in the stadium scenario. Thus, it is possible to directly compare the two scenarios in spite of there being different frequency bands and areas. In all simulations in the factory environment, each transmitting TRP has a UPA with N_{tx} = 256 antennas, and the user receiver side has N_{rx} = 16. Different numbers of transmitted symbols per subcarrier were considered in the simulations, and N_s = 3. When there are no active RIS panels in the factory, there are only two BSs, each with three sectors, making a total of six sectors. In this case, users are uniformly distributed within a radius of 70 m (see Table 3). When simulating performance curves with BSs and RISs operating simultaneously, users that are connected to BSs will be uniformly distributed within a radius of 50 m. Some 16 RIS panels are uniformly distributed inside the scenario, and users served by them are distributed within a radius of 25 m.

In Figure 14, the throughput performance versus N_u in the factory scenario is shown, with low BS antenna height and RIS panels, for two different resource blocks. The scenario parameters are N_{tx} = 256, N_{rx} = 16, N_s = 3. An assignment of 11 PRBs per user gives N_c = 132, and 25 PRBs per user gives N_c = 300. With 11 PRBs per user, 3300/120 = 25 is the number of users per sector. With 25 PRBs per user, 3300/3000 = 11 is the number of users per sector. As there are six sectors in the Factory, and the total number of users is 150 or 66 for 11 PRBs and 25 PRBs, respectively. When users are exclusively served by the TRPs of BSs with direct links, i.e., 100%BS + 0%RIS, we have a total throughput of approximately

41 Gbps for 150 users (pink line), and a total throughput of 37 Gbps for 66 users (red line). In the factory, there are 16 × 3 = 48 RIS panels and 2 × 3 = 6 TRPs (one per sector). When users at cell borders start to be served by RIS panels, 48 users must be subtracted, resulting in 150 – 48 = 102 users served by six TRPs. The 48 users are served by RIS 48/150 = 0.32 (blue lines), and the remaining 68% users are served by TRPs 68%BS + 32%RIS,11RB. In the case of 25 PRB (black lines), the total number of users is 66; we have 48 users served by RIS (i.e., 48/66 = 0.73) and the remaining 66 – 48 = 18 users served by TRPs (i.e.,18/66 = 0.27), 27%BS + 73%RIS,25RB. We observed that increasing the number of RIS panels from 576 up to 2304 only increases the throughput slightly. This increment is more noticeable for 25RB. In the case of the maximum number of users, there is almost no difference in the achieved throughput between lines 27%BS + 73%,25RB and 68%BS + 32%RIS,11RB. When compared to lines 100%BS + 0%RIS, the throughput gains are between 29% for 11 PRBs and 53% for 25 PRBs.

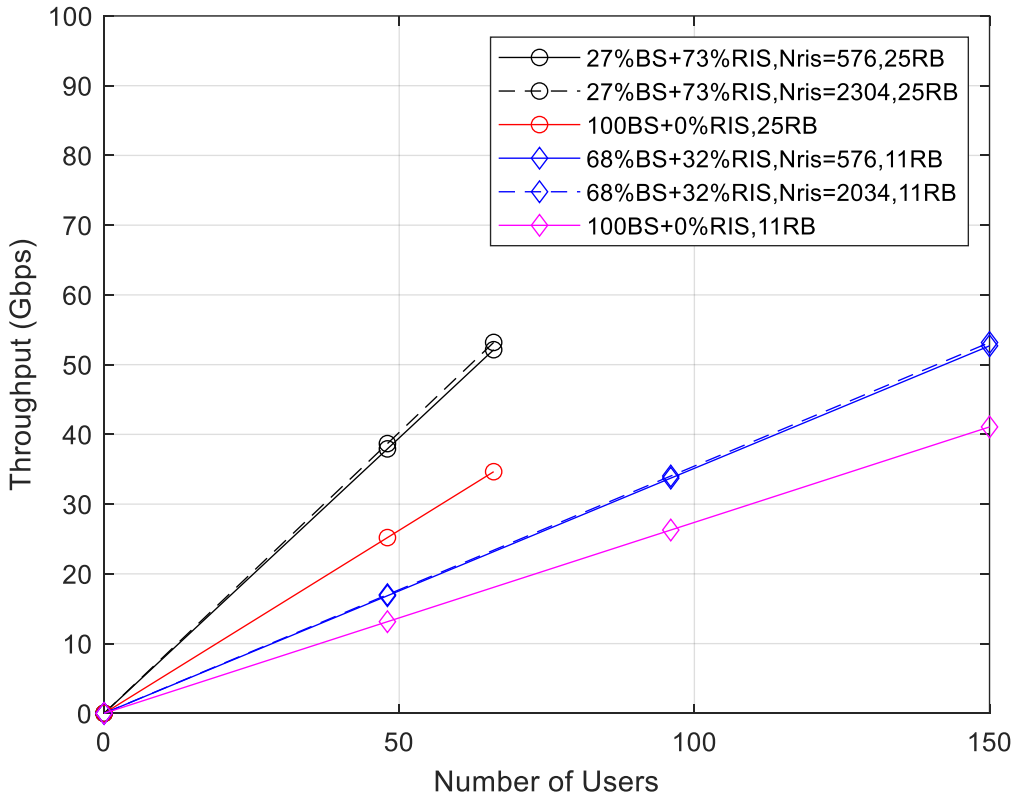

Figure 14. Throughput vs. number of users for the factory scenario for two different resource blocks, and RIS panels. N_{tx} = 256, N_{rx} = 16, N_s = 3 (low BS antenna height and P_{tx} = 30 mW).

Figure 15 presents the average coverage versus transmitted power for both N_c = 132 (11 PRB) and N_c = 300 (25 PRB), with a maximum transmitted power of 30 mW (14.8 dBm), corresponding to the throughput performance illustrated in Figure 14. As expected, there is a direct correspondence between the throughput performance of Figure 14 and the associated coverage of Figure 15. In terms of performance of coverage, the differences between 11 PRBs or 25 PRBs per user are higher than with throughput. We observed that for 11 PRBs with the maximum transmitted power, a highest coverage of 99% was achieved for both 576 and 2304 RIS panels. However, the coverage for 25 PRBs per user is higher when the RIS panels have 2304 elements compared to 576 elements, not only for 30 mW, but also for all transmitted power intervals. The lowest coverage values are 67% and 77%, corresponding both to non-activated RIS panels, i.e., 100%BS + 0%RIS,25RB and 100%BS + 0%RIS,11RB, respectively. The corresponding coverage gains are between 29% for 11 PRBs and 48% for 25 PRBs. This is in accordance with throughput values of Figure 13.

The average coverage of the factory scenario (Figure 15) is slightly higher than the coverage of the stadium scenario (Figure 12).

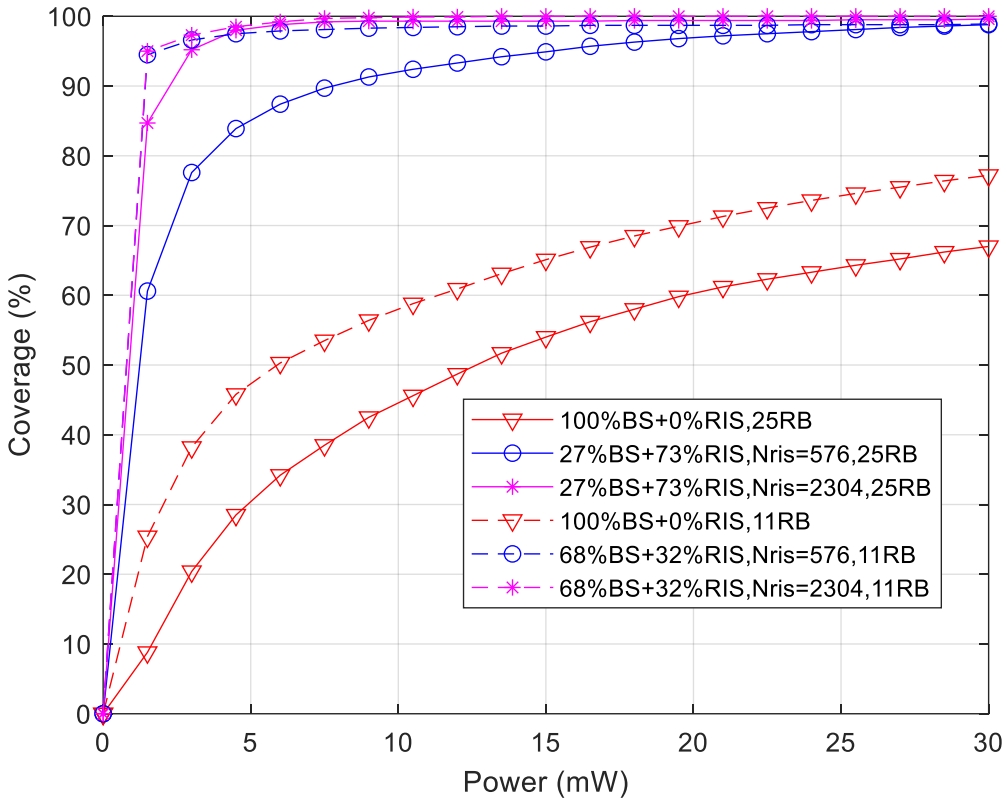

Figure 15. Coverage vs. transmission power for the factory scenario for N_{tx} = 256, N_{rx} = 16, with two different numbers of resource blocks and RIS panels.

In Figure 16, we consider the factory scenario, illustrating the aggregate throughput for each sector versus the number of PRBs per user, considering the maximum transmit power of 14.8 dBm. We evaluate the sector throughput for a specific number of PRBs, namely, 1 PRB, 5 PRBs, 11 PRBs, 18 PRBs and 25 PRBs. A total of 1 PRB per user resulted in N_c = 12, with 5 PRBs per user resulting in N_c = 60, and 11 PRBs per user resulting in N_c = 132. A total of 18 PRBs per user resulted in N_c = 216, and finally, 25 PRBs per user resulted in N_c = 300 subcarriers. The number of users per sector when each user has 1 PRB is 3300/12 = 275. In total, there are six sectors in the stadium; thus, there were a maximum of 1650 active users. For the case wherein every active user has 25 PRBs, there are 3300/300 = 11 users per sector, and the total number of active users in the factory is 66. We observe in Figure 15 that for the red curve LBS (100%BS + 0%RIS) where the BS UPA antenna is at 2 m height, there is a maximum throughput for 1 PRB, which is the same for both curves: BS + RIS (black) and HBS (pink). For 5 PRBs, 11 PRBs, and 18 PRBs per user, there is a clear linear decrease in the throughput of the red curve compared to the black curve (BS + RIS), which has almost the same constant throughput. The decrease in throughput continues with 25 PRBs, but in a slower way. The pink curve HBS with the BS UPA antenna at 8 m height also has a decreasing aggregate throughput per sector for an increasing number of PRBs. However, there is only a very slight decrease with the increasing number of PRBs. When users are served by a BS at 8 m height, there is almost no interference from the high clutter density because the height of clutter is 6 m. The reason that transmitting higher number of PRBs per user decreases the throughput has to do with packets of large size that are more likely to suffer deep fades. The link diversity of RIS + BS is provided by the C-RAN operation that is able to prevent a decrease in throughput.

Therefore, if possible, the antennas of BS should be placed as high as possible so that they are above the height of the high clutter density characteristic of indoor factory scenarios.

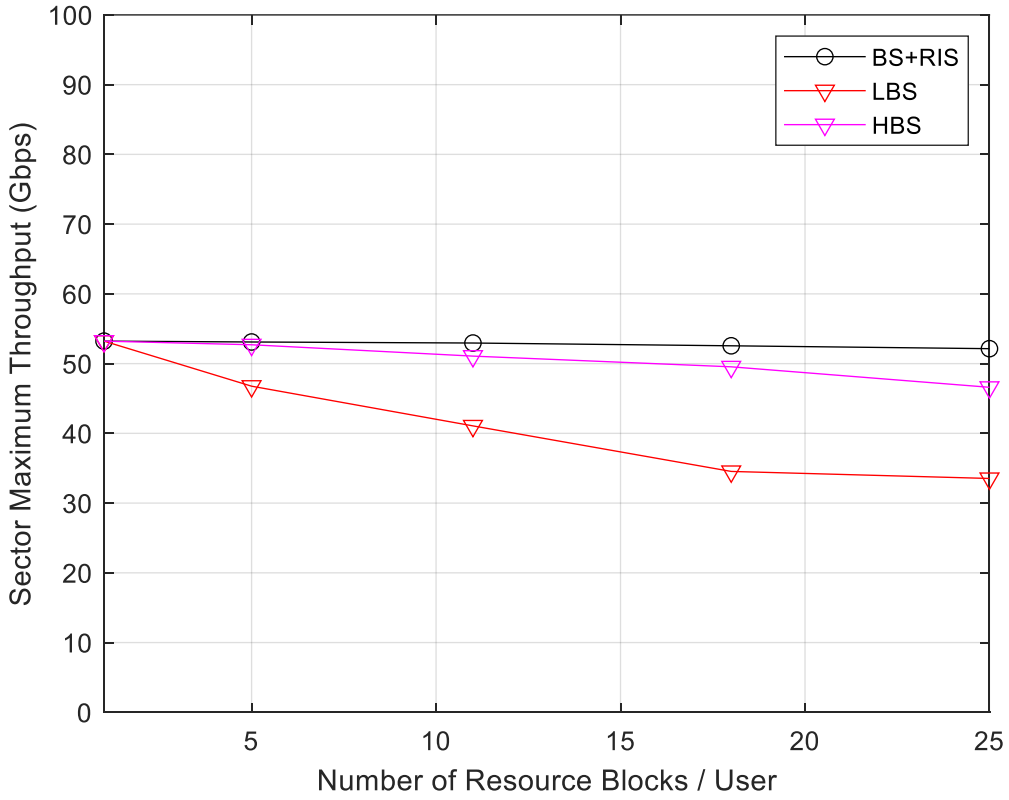

Figure 16. Throughput vs. number of resource blocks per user for the factory scenario (LBS with BS antenna height 2 m, HBS with BS antenna height 8 m, maximum sector load, N_{tx} = 256, N_{rx} = 16 and N_{ris} = 2304).

The comparison of Figure 16 with Figure 13 indicates that the aggregate throughput of each sector of the factory is half of the throughput of the stadium. This is explained by the number of BSs in the factory being half of the number in the stadium. Therefore, if we need to increase the aggregate throughput of the factory scenario, we have two option: (1) we can increase the number of BSs, or (2) we can use carrier aggregation. Indeed, 5G NR allows for the aggregation of 16 carriers, each one with 400 MHz. At 100 GHz, it is possible to have available a total bandwidth of 6.4 GHz. The first solution involves densification of the network, and it is not possible to achieve energy efficiency with this solution. To be energy-efficient and achieve high sector throughput, we need to aggregate carriers and place RIS surfaces distributed around the BSs of the scenario.

4. Conclusions

RISs are considered a key technology for future wireless networks, in particular for B5G and 6G systems. In this article, we present an approach to increase the energy efficiency of future networks by replacing BS with RIS panels considering multi-stream multiple-input–multiple-output (MIMO)–orthogonal frequency division multiplexing (OFDM) links. We perform system-level assessments of RIS-aided B5G C-RAN scenarios operating in 3.6 GHz, mmWave (28 GHz), and sub-THz (100 GHz) bands. We have only considered scenarios wherein communication for/from different users is based on orthogonal multiple access, avoiding intra-cell interference.

We have addressed smart radio environments and the task of increasing their capacity, for example, assessing the number of active IoT devices in a smart city scenario, in 3.6 GHz and 28 GHz. The minimum number of active users in the smart city environment depends

on the coherence interval of the scenario because of the need for orthogonal reference pilots in the uplink. We considered 19,800 transmitting IoT devices, each one with one subcarrier per subframe of a 1 millisecond duration. The use of a C-RAN allows for decreasing the pilot pollution between sectors because of its operation mode. The introduction of RIS elements at 28 GHz in this scenario was able to increase the coverage of low-power and low-rate IoT devices located at cell borders. The coverage gain was about 7%.

In the other smart scenarios evaluated, namely, the outdoor/indoor stadium with pitch scenario at 28 GHz and the indoor factory at 100 GHz, we studied the improvement in terms of coverage and throughput.

The maximum number of evaluated active users in the stadium with pitch scenario was 3300, transmitting one PRB with 12 subcarriers each. We have evaluated the effect of variations in BS transmission power from 24 dBm up to 35 dBm, concluding that the performance results are almost constant. The introduction of C-RAN, in spite of its higher computing complexity, allowed for decreasing inter-cell interference between sectors. Throughput and coverage gains between 97% and 110% were observed with the introduction of RIS at cell borders of the BS on the stadium turf and in the stands. However, the throughput and coverage gains depend on the number of PRBs per user. The gains are higher when increasing the number of PRBs per user.

The maximum number of active users in the indoor factory was 1650, assuming that one PRB per user was transmitted. We have evaluated different numbers of RIS elements, from 576 up to 2304, concluding that the difference in performance is small. However, for an increasing number of PRBs per user, the higher performance of RIS with 2304 elements was noticeable. Throughput and coverage gains are between 29% and 50%, depending on the number of PRBs per user. To increase throughput, the antennas of BS should be placed higher than the height of clutter density in the factory. We proposed the use of carrier aggregation of up to 16 carriers, each with 400 MHz, in order to increase the throughput in this scenario at 100 GHz.

In future work, we intend to apply new semi-deterministic path loss models which are capable of accurately predicting path loss in scenarios with more obstructions and irregular layouts of factories at 300 GHz (THz band), in order to evaluate coverage and throughput performance, using system-level simulations.

Author Contributions: Conceptualization, V.V., J.P.P., N.S. and A.C.; methodology, V.V., J.P.P., N.S. and A.C.; software, V.V., J.P.P., N.S. and A.C; validation, V.V., J.P.P., N.S. and A.C.; formal analysis, V.V., J.P.P., N.S. and A.C.; investigation, V.V., J.P.P., N.S., M.M.d.S. and A.C.; resources, A.C. and N.S.; data curation, V.V., J.P.P., N.S. and A.C.; writing—original draft preparation, V.V., J.P.P., N.S., M.M.d.S. and A.C.; writing—review and editing, V.V., J.P.P., M.M.d.S., N.S. and A.C.; visualization, V.V., J.P.P., N.S. and A.C.; supervision, A.C. and N.S.; project administration, A.C. and N.S.; funding acquisition, A.C., N.S. and M.M.d.S. All authors have read and agreed to the published version of the manuscript.

Funding: The authors acknowledge the funding provided by FCT/MCTES through national funds, and when applicable, they also acknowledge EU funds under the project UIDB/50008/2020.

Institutional Review Board Statement: Not applicable.

Informed Consent Statement: Not applicable.

Data Availability Statement: The data presented in this study are available on request from the corresponding author. The data are not publicly available due to privacy.

Conflicts of Interest: The authors declare no conflicts of interest.

References

1. Wong, V.W. *Key Technologies for 5G Wireless Systems*; Cambridge University Press: Cambridge, UK, 2017; ISBN 9781107172418.
2. 3rd Generation Partnership Project (3GPP). TS 38.101 v14.1.1, 5GNR. User Equipment (UE) Radio Transmission and Reception, Release 15, August 2017. Available online: https://3gpp.org/ftp/Specs/archive/38_series/38.101-1/38101-1-001.zip (accessed on 23 January 2022).
3. Marques da Silva, M.; Dinis, R. Power-Ordered NOMA with Massive MIMO for 5G Systems. *Appl. Sci.* **2021**, *11*, 3541. [CrossRef]

4. Nidhi, A.; Mihovska, R.; Prasad, R. Overview of 5G New Radio and Carrier Aggregation: 5G and Beyond Networks. In Proceedings of the 2020 23rd International Symposium on Wireless Personal Multimedia Communications (WPMC), Okayama, Japan, 19–26 October 2020; pp. 1–6.
5. Farris, I.; Taleb, T.; Khettab, Y.; Song, J. A survey on emerging SDN and NFV security mechanisms for IoT systems. *IEEE Commun. Surv. Tutor.* **2018**, *21*, 812–837. [CrossRef]
6. Xu, L.D.; He, W.; Li, S. Internet of Things in industries: A survey. *IEEE Trans. Ind. Inform.* **2014**, *10*, 2233–2243. [CrossRef]
7. Brundu, F.G.; Patti, E.; Osello, A.; Del Giudice, M.; Rapetti, N.; Krylovskiy, A.; Jahn, M.; Verda, V.; Guelpa, E.; Rietto, L.; et al. IoT software infrastructure for energy management and simulation in smart cities. *IEEE Trans. Ind. Inform.* **2017**, *13*, 832–840. [CrossRef]
8. Lee, B.M.; Yang, H. Massive MIMO for industrial Internet of Things in cyber-physical systems. *IEEE Trans. Ind. Inform.* **2018**, *14*, 2641–2652. [CrossRef]
9. Lee, B.M.; Yang, H. Massive MIMO with Massive Connectivity for Industrial Internet of Things. *IEEE Trans. Ind. Electron.* **2020**, *67*, 5187–5196. [CrossRef]
10. Björnson, E.; Wymeersch, H.; Matthiesen, B.; Popovski, P.; Sanguinetti, L.; de Carvalho, E. Reconfigurable Intelligent Surfaces: A signal processing perspective with wireless applications. *IEEE Signal Process. Mag.* **2022**, *39*, 135–158. [CrossRef]
11. Yang, F.; Pitchappa, P.; Wang, N. Terahertz Reconfigurable Intelligent Surfaces (RISs) for 6G Communication Links. *Micromachines* **2022**, *13*, 285. [CrossRef]
12. Velez, V.; Pavia, J.P.; Souto, N.; Sebastião, P.; Correia, A. Performance Assessment of a RIS-empowered post-5G/6G network operating at the mmWave/THz bands. *IEEE Access* **2023**, *11*, 49625–49638. [CrossRef]
13. Zaidi, S.; Smida, O.B.; Affes, S.; Vilaipornsawai, U.; Zhang, L.; Zhu, P. User-Centric Base-Station Wireless Access Virtualization for Future 5G Networks. *IEEE Trans. Commun.* **2019**, *67*, 5190–5202. [CrossRef]
14. 3rd Generation Partnership Project (3GPP). TR 38.913 5G.; Study on Scenarios and Requirements for Next Generation Access Technologies, Version 16.0.0 Release 16, July 2020. Available online: https://3gpp.org/ftp/Specs/archive/38_series/38.913/38913-g00.zip (accessed on 1 November 2023).
15. 3rd Generation Partnership Project (3GPP). TR 38.901 Study on Channel Model for Frequencies from 0.5 to 100 GHz, Version 16.1.0, Release 16. November 2020. Available online: https://3gpp.org/ftp/Specs/archive/38_series/38.901/38901-e20.zip (accessed on 1 November 2023).
16. 3rd Generation Partnership Project (3GPP). TS 38.211 v15.2.0. 5G/NR Physical Channels and Modulation, (Release 15). 2018. Available online: https://3gpp.org/ftp/Specs/archive/38_series/38.211/38211-f30.zip (accessed on 1 November 2023).
17. 3rd Generation Partnership Project (3GPP). TS 38.214; NR.; Physical Layer Procedures for Data, (Release 15). 2020. Available online: https://3gpp.org/ftp/Specs/archive/38_series/38.214/38214-fb0.zip (accessed on 1 November 2023).
18. 3rd Generation Partnership Project (3GPP). TS 38.213; NR.; Physical Layer Procedures for Control, (Release 15). 2020. Available online: https://3gpp.org/ftp/Specs/archive/38_series/38.213/38213-fb0.zip (accessed on 1 November 2023).
19. Zaidi, A.A.; Baldemair, R.; Tullberg, H.; Bjorkegren, H.; Sundstrom, L.; Medbo, J.; Kilinc, C.; Da Silva, I. Waveform and Numerology to Support 5G Services and Requirements. *IEEE Commun. Mag.* **2016**, *54*, 90–98. [CrossRef]
20. Begishev, V.; Samuylov, A.; Moltchanov, D.; Machnev, E.; Koucheryavy, Y.; Samouylov, K. Connectivity Properties of Vehicles in Street Deployment of 3GPP NR Systems. In Proceedings of the 2018 IEEE Globecom Workshops (GC Wkshps), Abu Dhabi, United Arab Emirates, 9–13 December 2018.
21. Gkonis, P.K.; Trakadas, P.T.; Kaklamani, D.I. A Comprehensive Study on Simulation Techniques for 5G Networks: State of the Art Results, Analysis, and Future Challenges. *Electronics* **2020**, *9*, 468. [CrossRef]
22. ElMossallamy, M.A.; Zhang, H.; Song, L.; Seddik, K.G.; Han, Z.; Li, G.Y. Reconfigurable Intelligent Surfaces for Wireless Communications: Principles, Challenges, and Opportunities. *IEEE Trans. Cogn. Commun. Netw.* **2020**, *6*, 990–1002. [CrossRef]
23. Praia, J.; Pavia, J.P.; Souto, N.; Ribeiro, M. Phase Shift Optimization Algorithm for Achievable Rate Maximization in Reconfigurable Intelligent Surface-Assisted THz Communications. *Electronics* **2021**, *11*, 18. [CrossRef]
24. Zhang, S.; Zhang, R. Capacity Characterization for Intelligent Reflecting Surface Aided MIMO Communication. *IEEE J. Sel. Areas Commun.* **2020**, *38*, 1823–1838. [CrossRef]
25. Huang, C.; Alexandropoulos, G.C.; Zappone, A.; Debbah, M.; Yuen, C. Energy Efficient Multi-User MISO Communication Using Low Resolution Large Intelligent Surfaces. In Proceedings of the 2018 IEEE Globecom Workshops (GC Wkshps), Abu Dhabi, United Arab Emirates, 9–13 December 2018; pp. 1–6. [CrossRef]
26. Mu, X.; Liu, Y.; Guo, L.; Lin, J.; Al-Dhahir, N. Capacity and Optimal Resource Allocation for IRS-Assisted Multi-User Communication Systems. *IEEE Trans. Commun.* **2021**, *69*, 3771–3786. [CrossRef]
27. Pavia, J.P.; Velez, V.; Ferreira, R.; Souto, N.; Ribeiro, M.; Silva, J.; Dinis, R. Low Complexity Hybrid Precoding Designs for Multiuser mmWave/THz Ultra Massive MIMO Systems. *Sensors* **2021**, *21*, 6054. [CrossRef] [PubMed]
28. Pei, X.; Yin, H.; Tan, L.; Cao, L.; Li, Z.; Wang, K.; Zhang, K.; Björnson, E. RIS-Aided Wireless Communications: Prototyping, Adaptive Beamforming, and Indoor/Outdoor Field Trials. *IEEE Trans. Commun.* **2021**, *69*, 8627–8640. [CrossRef]
29. Lavdas, S.; Gkonis, P.K.; Zinonos, Z.; Trakadas, P.; Sarakis, L. An Adaptive Hybrid Beamforming Approach for 5G-MIMO mmWave Wireless Cellular Networks. *IEEE Access* **2021**, *9*, 127767–127778. [CrossRef]
30. Gkonis, P.K. A Survey on Machine Learning Techniques for Massive MIMO Configurations: Application Areas, Performance Limitations and Future Challenges. *IEEE Access* **2023**, *11*, 67–88. [CrossRef]

31. Liu, S.; Ni, P.; Liu, R.; Liu, Y.; Li, M.; Liu, Q. BS-RIS-User Association and Beamforming Designs for RIS-aided Cellular Networks. In Proceedings of the 2021 IEEE/CIC International Conference on Communications in China (ICCC), Xiamen, China, 28–30 July 2021; pp. 563–568. [CrossRef]
32. Sihlbom, B.; Poulakis, M.I.; Renzo, M.D. Reconfigurable Intelligent Surfaces: Performance Assessment Through a System-Level Simulator. *IEEE Wirel. Commun.* **2022**, *30*, 98–106. [CrossRef]
33. Gu, Q.; Wu, D.; Su, X.; Wang, H.; Cui, J.; Yuan, Y. System-level Simulation of Reconfigurable Intelligent Surface assisted Wireless Communications System. *arXiv* **2022**, arXiv:2206.14777. [CrossRef]
34. Rappaport, T.S. *Wireless Communications: Principles and Practice*, 2nd ed.; Englewood Cliffs: Prentice-Hall, NJ, USA, 2002.